HHS Public Access

Author manuscript

Nature. Author manuscript; available in PMC 2018 February 26.

Published in final edited form as:

Nature. 2017 June 22; 546(7659): 544–548. doi:10.1038/nature22819.

Histone Deacetylase 3 Prepares Brown Adipose Tissue For Acute Thermogenic Challenge

Matthew J. Emmett[1,2,*], **Hee-Woong Lim**[1,3,*], **Jennifer Jager**[1,2], **Hannah J. Richter**[1,2], **Marine Adlanmerini**[1,2], **Lindsey C. Peed**[1,2], **Erika R. Briggs**[1,2], **David J. Steger**[1,2], **Tao Ma**[4], **Carrie A. Sims**[1,5], **Joseph A. Baur**[1,6], **Liming Pei**[1,7], **Kyoung-Jae Won**[1,3], **Patrick Seale**[1,8], **Zachary Gerhart-Hines**[4], and **Mitchell A. Lazar**[1,2,3]

[1]Institute for Diabetes, Obesity, and Metabolism, Perelman School of Medicine at the University of Pennsylvania, Philadelphia, PA 19104, USA

[2]Division of Endocrinology, Diabetes, and Metabolism, Department of Medicine, Perelman School of Medicine at the University of Pennsylvania, Philadelphia, PA 19104, USA

[3]Department of Genetics, Perelman School of Medicine at the University of Pennsylvania, Philadelphia, PA 19104, USA

[4]Section for Metabolic Receptology at the Novo Nordisk Foundation Center for Basic Metabolic Research, and Institute for Neuroscience and Pharmacology, University of Copenhagen, Copenhagen, 2200, DK

[5]The Trauma Center at Penn, Department of Surgery, Perelman School of Medicine at the University of Pennsylvania, Philadelphia, PA 19104

[6]Department of Physiology, Perelman School of Medicine at the University of Pennsylvania, Philadelphia, PA 19104, USA

[7]Center for Mitochondrial and Epigenomic Medicine, Children's Hospital of Philadelphia, and Department of Pathology and Laboratory Medicine, Perelman School of Medicine at the University of Pennsylvania, Philadelphia, PA 19104, USA

[8]Department of Cell and Developmental Biology, Perelman School of Medicine at the University of Pennsylvania, Philadelphia, PA 19104, USA

Address correspondence to: Mitchell A. Lazar, M.D., Ph.D.: lazar@mail.med.upenn.edu.

*These authors contributed equally to this work.

Correspondence and requests for materials should be addressed to M.A.L. (lazar@mail.med.upenn.edu).

Contributions

M.J.E., M.A.L. conceived the project, designed experiments, analyzed results, and wrote the manuscript; M.J.E. performed animal experiments, immunoblots, RNA-seq, and ChIP-seq; M.J.E., J.J. performed GRO-seq; H.W.L., K.J.W. performed bioinformatic analyses; C.A.S., M.J.E performed mitochondrial assays. M.J.E, H.J.R. performed cellular experiments. M.A. performed endogenous co-immunoprecipitation. D.J.S. performed H3/H3Kme1 ChIP-seq. L.C.P., E.R.B. provided animal husbandry and technical assistance. T.M., Z.G.H., P.S., J.A.B., L.P. provided reagents and experimental design. All authors read and commented on the manuscript.

Sequencing data have been deposited in the Gene Expression Omnibus (GEO), GSE83928.

The authors declare no competing financial interests.

Abstract

Brown adipose tissue (BAT) is a thermogenic organ that dissipates chemical energy as heat to protect animals against hypothermia and to counteract metabolic disease[1]. However, the transcriptional mechanisms that determine BAT thermogenic capacity prior to environmental cold are unknown. Here we show that Histone Deacetylase 3 (HDAC3) is required to activate BAT enhancers to ensure thermogenic aptitude. Mice with BAT-specific genetic ablation of HDAC3 become severely hypothermic and succumb to acute cold exposure. UCP1 is nearly absent in BAT lacking HDAC3 and there is also marked down-regulation of mitochondrial oxidative phosphorylation (OXPHOS) genes resulting in diminished mitochondrial respiration. Remarkably, although HDAC3 acts canonically as a transcriptional corepressor[2], it functions as a coactivator of Estrogen-Related Receptor α (ERRα) in BAT. HDAC3 coactivation of ERRα is mediated by deacetylation of PGC-1α and is required for the transcription of *Ucp1*, *Pgc-1*α and OXPHOS genes. Importantly, HDAC3 promotes the basal transcription of these genes independent of adrenergic stimulation. Thus, HDAC3 uniquely primes *Ucp1* and the thermogenic transcriptional program to maintain a critical capacity for thermogenesis in BAT that can be rapidly engaged upon exposure to dangerously cold temperature.

BAT is a major site of mammalian non-shivering thermogenesis mediated through UCP1-dependent respiration[1]. Cold temperature triggers fuel oxidation and UCP1-mediated dissipation of the mitochondrial proton gradient to rapidly generate heat in BAT[1,3], and C57BL/6J (B6) mice acclimated to room temperature (22°C) survive acute exposure to 4°C through this mechanism[1,4]. While UCP1-deficient mice can utilize other thermogenic mechanisms upon gradual acclimation to cold[5,6,7,8], UCP1 is required to prevent lethal hypothermia upon rapid decreases in ambient temperature, such as from 22°C to 4°C[4]. Although much is known about brown adipose commitment and differentiation[9], the transcriptional mechanisms that ensure readiness of mature BAT for immediate heat production remain unclear[10].

The ubiquitously expressed class I histone deacetylase HDAC3 is an epigenomic modulator of nuclear receptor controlled gene expression, functioning as a stoichiometric component of the nuclear receptor corepressor (NCoR) complex[2] to modulate deacetylation of histones as well as non-histone targets[11]. Global HDAC3 deletion is embryonic lethal[12], but studies of its tissue-specific functions link HDAC3 to hepatic steatosis[13], macrophage function[14], atherosclerosis[15], bone density[16], intestinal homeostasis[17], and cardiac energy metabolism[18,19]. However, its physiological role in BAT is not known.

We bred B6 mice with a floxed HDAC3 allele to B6 mice harboring the pan-adipose *Adiponectin*-Cre (*Adipoq*-Cre) and the BAT-specific *Ucp1*-Cre for conditional pan-adipose and BAT-specific knockout (KO) (Extended Data Fig. 1a), and challenged adults with a drop in ambient temperature from 22°C to 4°C. As expected, control littermates maintained their core body temperature in the face of the acute environmental change (Fig. 1a). Strikingly, both the *Adipoq*-Cre and *Ucp1*-Cre HDAC3 KO mice exhibited a rapid loss of core body temperature, becoming severely hypothermic within just a few hours of moving to 4°C (Fig. 1a). The inability to maintain core body temperature was lethal for every mouse lacking HDAC3 in BAT, whereas all the control littermates survived (Fig. 1b). Notably, the severe

cold susceptibility of the HDAC3 KO mice was similar to that observed in congenic *Ucp1* KO mice (Figs. 1a–b).

The requirement for HDAC3 in regulating BAT-thermogenic capacity was examined by measuring norepinephrine (NE)-induced whole-body oxygen consumption in anesthetized mice. Control littermates exhibited a rapid and robust increase in oxygen consumption following NE treatment whereas HDAC3 KO mice had a blunted response comparable to that observed in *Ucp1* KO mice[1] (Fig. 1c). Despite severely impaired BAT metabolic respiration, loss of HDAC3 had little effect on interscapular BAT mass, BAT mitochondrial content, or total body mass (Extended Data 1b–d).

BAT mitochondrial function was tested by high-resolution respirometry. As expected, palmitoylcarnitine and pyruvate substrates induced robust respiration in BAT mitochondria from control mice, which was UCP1-dependent and inhibited by guanosine diphosphate (GDP)[1] (Fig. 1d). Remarkably, substrate-induced respiration was impaired in mitochondria from HDAC3 KO BAT, as was coupled respiration on substrates for Complexes I, II, or IV of the electron transport chain (Fig. 1d). Consistent with this mitochondrial dysfunction, histological analysis revealed the presence of larger lipid droplets in HDAC3 KO BAT (Fig. 1e). By contrast, the histology of inguinal white adipose tissue (iWAT) lacking HDAC3 was similar to that of wild type mice (Extended Data Fig. 1e),

To elucidate the molecular basis through which HDAC3 controls the thermogenic capacity of BAT, we next performed RNA-sequencing (RNA-seq) on BAT from control and KO mice housed at thermoneutrality (29°C) to avoid the potentially confounding influence of cold-stress. Consistent with the well-known function of HDAC3 as a corepressor, many genes were induced by loss of HDAC3, including classic repression targets of the nuclear receptor Rev-erbαsuch as *Bmal1 (Arntl)*, *E4BP4 (Nfil3)*, *Elovl5*, and *Plin2* (Fig. 2a). However, many genes were also decreased in HDAC3 KO BAT, including a near-complete loss of *Ucp1* in the BAT of HDAC3 KO animals (Fig. 2a). UCP1 protein expression was nearly undetectable in HDAC3 KO BAT, at both 29°C and 22°C (Fig. 2b). *Ucp1* expression remained low in HDAC3 KO BAT after acute cold exposure (Extended Data 2a–b) although it was induced in iWAT (Extended Data 2c–d), suggesting a BAT-selective requirement for HDAC3. BAT HDAC3 mRNA and protein levels were not appreciably affected by acute cold exposure (Extended Data 2e–f), and HDAC3 was neither induced nor required for primary brown adipocyte differentiation (Extended Data. 3a–d). However, primary brown adipocytes lacking HDAC3 exhibited reduced basal *Ucp1,* which was minimally responsive to isoproterenol (Extended Data 3e–g), demonstrating a cell autonomous effect of HDAC3.

Analysis of the genes repressed by HDAC3 KO in BAT revealed a strong enrichment for thermogenic pathways, including mitochondrial oxidative phosphorylation, tricarboxylic acid cycle (TCA) enzymes, and other metabolic and energy producing processes, with no signal for inflammatory pathways (Fig. 2c). Many components of the TCA cycle and complexes I–V of the electron transport chain were diminished in the absence of HDAC3 (Fig. 2d, Extended Data 4a), as confirmed by RT-qPCR at both 29°C and 22°C in pan-adipose as well as BAT-specific HDAC3 KO models (Extended Data 4b–c).

Relative to controls, BAT HDAC3 KO animals had similar body weight and lean mass, with slightly less body fat but indistinguishable basal energy expenditure, activity, and food intake at 22°C (Extended Data 5). Moreover, after 12 weeks of high fat feeding at room temperature, pan-adipose and BAT-specific HDAC3 KO mice gained similar amounts of weight and body fat relative to controls (Extended Data 6a–d), whose BAT HDAC3 expression was indistinguishable from normal chow fed mice (Extended Data 6e). These findings are similar to the phenotype of *Ucp1* KO mice[4], and suggestive of *Ucp1*-independent mechanisms that may control energy-expenditure and body weight[5,6,7,8]. Thus, HDAC3 is uniquely required for priming the mitochondrial oxidative and thermogenic energy-expending gene programs in classic BAT to defend against environmental cold.

To determine the mechanism by which HDAC3 drives expression of thermogenic gene pathways, we performed ChIP-seq in BAT for HDAC3 and for acetylated histone H3 lysine 27 (H3K27ac) as a marker of active enhancers[20]. Loss of HDAC3 led to reduced H3K27ac at many sites of HDAC3 binding in control mice, often near genes that were repressed by HDAC3-depletion (Fig. 3a). These results imply that, at these sites, the usual function of HDAC3 as a histone deacetylase was overridden by its function as a coactivator. By contrast, H3K27ac was increased at HDAC3 bound sites near genes that were induced in HDAC3 KO BAT (Fig. 3a).

Steady state mRNA levels correlated well with nascent transcription at gene bodies as assessed by Global Run-on Sequencing (GRO-seq)[21] (Extended Data 7a). Mining of the GRO-seq data for non-coding enhancer RNA (eRNA) transcription to map functional enhancers[22,23] revealed dramatic reduction in activity of multiple enhancers at the *Ucp1* locus (Fig. 3b). Genome-wide, HDAC3 binding at eRNAs which were down-regulated upon HDAC3 KO was enriched in BAT of control mice, adding to the evidence that HDAC3 functioned as a coactivator at these enhancers (Fig. 3c). Since *Rev-erbα* deletion has the opposite effect on *Ucp1*[24], we reason that the ability of HDAC3 to function as Rev-erbα corepressor must be overcome by HDAC3 coactivation of a different transcription factor.

To identify the transcription factor(s) coactivated by HDAC3, genome-wide *de novo* motif analysis was performed at sites of eRNA down-regulation in HDAC3 KO BAT, revealing enrichment of the binding motif for Estrogen-Related Receptors (ERR) at both 29°C and 22°C (Fig. 3d, Extended Data 7b). ERRs are potent activators of mitochondrial metabolism, OXPHOS pathways, and energy metabolism[25]. Other enriched motifs included those of known adipose lineage factors[26] including the BAT-specific EBF2[27]. Confirming the motif prediction, genome-wide ERRα binding in BAT was strongest at sites where eRNAs were down-regulated upon HDAC3 KO (Fig. 3e). On a genome-wide level HDAC3 and ERRα binding strongly co-localized along with NCoR at down-regulated enhancers (Fig. 3f), suggesting a novel function of HDAC3. Moreover, endogenous ERRα and HDAC3 co-immunoprecipitated in mature brown adipocytes (Extended Data Fig. 7c).

Inspection of the *Ucp1* locus revealed a super-enhancer (encompassing the eRNAs highlighted in Fig. 3b) at sites of co-localized HDAC3 and ERRα (Fig. 3g). Absence of HDAC3 led to marked attenuation of eRNA transcription and decreased levels of H3K27ac (Fig. 3g, Extended Data 7d–e), along with dramatic reduction of *Ucp1* mRNA at 29°C and

22°C in both HDAC3 KO models (Fig. 3g, Extended Data 7f). Loss of HDAC3 had little or no effect on ERRα binding at the *Ucp1* locus (Fig. 3g, Extended Data 7g). Genetic ablation of ERRαdecreased *Ucp1* expression and eRNA transcription in BAT (Extended Data 7h–i) as well as in mature brown adipocytes (Extended Data 7j), albeit to a lesser degree than HDAC3 KO perhaps due to redundancy with ERRγ[28]. These data strongly suggest that HDAC3 is a critical coactivator of ERR-driven thermogenic gene transcription in BAT.

Transcriptional activation by ERRα is highly dependent upon the coactivator peroxisome proliferator-activated receptor gamma coactivator 1 alpha (*Pgc-1α,* also known as *Ppargc1α*)[25,29]. Notably, the transcriptional function of PGC-1α is activated by lysine deacetylation[29], suggesting the possibility that HDAC3 may activate ERR-dependent transcription via deacetylation of PGC-1α. Indeed, HDAC3 markedly increased the transcriptional activity of ERRα at a major HDAC3-bound enhancer of the *Ucp1* gene in the presence of wild type PGC-1α but not a mutant form of PGC-1α that is unable to directly interact with ERRα (Fig. 4a). Both PGC-1α and HDAC3 co-immunoprecipitated with ERRα (Extended Data Fig. 8a), and HDAC3 robustly deacetylated PGC-1α that had been acetylated by the histone acetyltransferase GCN5[29], both in cells and *in vitro*, and in a manner that was prevented by the class I HDAC inhibitor trichostatin A (TSA) (Figs. 4b–c). HDAC3 also reversed GCN5-mediated repression of PGC-1α coactivator function (Extended Data 8b). Moreover, ectopic expression of non-acetylatable but not wild type PGC-1α in primary brown adipocytes lacking HDAC3 (Extended Data 8c) markedly induced expression of *Ucp1* but not the adipocyte differentiation marker *Fasn* (Extended Data 8d).

In addition to the post-translational regulation of PGC-1α, the *Pgc-1α* genomic locus was bound by HDAC3 and ERRα at sites of potent enhancer activity that were lost in the absence of HDAC3 (Fig. 4d), and HDAC3 functioned as an activator at this enhancer (Fig. 4e). Indeed, *Pgc-1α* mRNA and protein were markedly reduced in HDAC3 KO BAT (Figs. 4f–g). Of note, combined deficiency of *Pgc-1α* and *Pgc-1β* leads to loss of BAT *Ucp1* expression and impaired mitochondrial function[30] reminiscent of the BAT HDAC3 KO phenotype. Enhancers at the gene encoding PGC-1β were also bound by HDAC3 and ERRα (Extended Data 9a), and *Pgc-1β* mRNA was markedly reduced in HDAC3 KO BAT (Extended Data 9b). Moreover, eRNAs at these sites were dependent upon HDAC3 (Extended Data 9c–d). Further, depletion of PGC-1α and β and/or ERRα in mature brown adipocytes cooperatively decreased *Ucp1* transcription (Extended Data 9e). Thus, the ability of HDAC3 to activate PGC-1α both transcriptionally and post-translationally amplifies its coactivator function at ERR-family regulated enhancers in a feed-forward manner (Fig. 4h).

Intriguingly, the transcription of *Ucp1* and *Pgc-1α* was even lower in the HDAC3 KO fat at thermoneutrality than at room temperature (Extended Data 9f), indicating that the effect of loss of HDAC3 on basal expression of these genes is more potent than eliminating sympathetic stimulation of BAT. This pattern of expression (HDAC3 KO<TN<RT) was identified in many additional genes (Fig. 4i) critical for oxidative phosphorylation and energy metabolism (Figure 4i–j). Thus, a critical function of HDAC3 in BAT is to maintain a minimal basal expression of *Ucp1* and other genes regulating energy metabolism.

The maintenance and protection of core body temperature through tight control of metabolism is a defining element of mammalian physiology. Our finding that BAT HDAC3 transcriptionally maintains the basal activity of thermogenic gene networks provides a physiological basis for the ability to rapidly generate heat in response to acute exposure to dangerously cold environmental temperatures. HDAC3 has a unique role in priming the brown adipocyte to support immediate thermogenic respiration and heat production without delay. Thus, distinct from adaptive (inducible) thermogenic mechanisms that require time to develop and respond, HDAC3 sets a basal thermogenic tone which establishes the facultative capacity of BAT to turn on rapidly, on-demand, to ensure readiness against acute and life-threatening cold exposure.

METHODS

Statistical Methods and Reproducibility

Data are presented as mean ± s.e.m. unless otherwise stated. Graphpad Prism software was utilized for graphing and statistical analysis. All statistical tests are fully described in figure legends and met criteria for normal distribution with similar variance. No statistical methods were utilized to pre-determine sample size. For comparison between two groups, a Student's *t*-test was utilized. For assessment between more than two groups, one-way ANOVA with multiple comparisons were utilized, and for assessment between two independent variables two-way ANOVA with multiple comparisons were utilized, followed by a Tukey or Holm-Sidak post-test. For survival analysis, a log-rank (Mantel-Cox) test was performed. False discovery rate (FDR) for RNA-seq analysis were calculated by EdgeR bioinformatics software. Experiments independently repeated three or more times: (Figures 1a–b, 2b, 3c (ChIP), 3e (ChIP), 4a–b, 4e–f, Ext. 1b, 3a–g, 7f, 7j, 8b, 9b–c). Experiments independently repeated two times: (Figures 1d–e, 4c, 4g, Ext. 1a, 1c–e, 2a–f, 5a, 5c–n, 7c, 7g, 8a, 8d). Experiments performed once: (Figure 1c, 2a (RNA-seq), 3a–b (ChIP-seq, GRO-seq), 3c (ChIP-seq), 3e (ChIP-seq), Ext. 4b–c, 5b, 6a–e, 7d–e, 7h–i, 9c–d).

Animal Studies

Animal experiments were performed according to ethical regulations and protocols approved by the Institutional Animal Care and Use Committee (IACUC) of the Perelman School of Medicine at the University of Pennsylvania and the Children's Hospital of Philadelphia. Mice were group housed with enrichment in a temperature and humidity controlled, specific-pathogen free animal facility at 22°C under a 12:12-h light-dark cycle with free access to standard chow (LabDiet, 5010) and water. High fat diet studies were conducted by feeding mice a purified-ingredient diet composed of 60:20:20 kcal percentage of fat/carbohydrate/protein (Research Diets, D12492) at twelve weeks of age. All experiments used male age-matched littermates group housed at 4–5 animals per cage. Gene expression and protein studies were carried out on 10–12-week-old male mice at ZT 10. Thermoneutrality and cold-exposure experiments were performed in climate-controlled rodent incubators (Powers Scientific) maintained at 29°C or 4°C to 5°C, respectively, with interior temperature monitoring by digital thermometers. For thermoneutrality experiments, mice were allowed to acclimate to 29°C for two weeks. No animals were excluded from studies and no randomization nor blinding was performed.

HDAC3$^{loxP/loxP}$ mice maintained on a C57BL/6 background were bred to *Adiponectin*-Cre[31] mice maintained on a C57BL/6J background (Jackson Labs, B6;FVB-Tg(Adipoq-Cre)1Evdr/J, Stock 010803), to a *Ucp1*-Cre maintained on a C57BL/6J background (Jackson Labs, B6.FVB-Tg(Ucp1-Cre)1Evdr/J, Stock 024670), and to *Rosa26*-CreER^{T2} mice maintained on a C57BL/6J background (Jackson Labs, B6.129-*Gt(Rosa)26Sor*$^{Tm1(cre/ERT2)Tyj}$/J, Stock 008463). *Ucp1*$^{-/+}$ mice maintained on a C57BL/6J background (Jackson Labs, B6.129-Ucp1tm1Kz/J, Stock 003124) were used to generate *Ucp1*$^{-/-}$ and *Ucp1*$^{+/+}$ mice. ERRα$^{\sim -+}$ mice maintained on a C57BL/6 background were used to generate ERRα$^{\sim --}$ and ERRα$^{+\sim +}$ mice as previously described[32]. Tissue-specific HDAC3 KO mice were generated by mating males heterozygous for *Adipoq*-Cre or *Ucp1*-Cre and homozygous for the floxed HDAC3 alelle to females homozygous for the HDAC3 allele. Male littermate Cre-positive (HDAC3 KO) and Cre-negative (littermate controls) mice were then group housed upon weaning.

Core Body Temperature Measurements and Cold-Tolerance Testing

Baseline measurements of internal core-body temperatures were recorded on 10 week-old male mice maintained at 22°C (starting at ZT 4) using a digital thermometer (Oakton Instruments, Temp 10T Thermocouple) and rectal thermocouple probe (Physitemp, RET-3 probe). Cold-exposure studies were performed within climate-controlled rodent incubators. Mice were placed in pre-chilled cages at 4–5°C with bedding, a cotton nestlet, free access to standard chow and water, and cage lid partially open. Rectal temperatures were recorded every 60 minutes. Individual mice were removed from the study and euthanized if core body temperature fell ≥10°C from baseline measurement. Core temperatures ≥10°C from baseline measurement were not included in core temperature analysis and scored as an event for survival analysis.

Whole-Animal Oxygen-Consumption Rate

Oxygen-consumption rates of 10 week-old male mice were measured using Comprehensive Laboratory Animal Monitoring System (CLAMS, Columbus Instruments) metabolic cages housed within environment-controlled rodent incubators. Following previously described protocols[33], mice maintained at 22°C were anesthetized with 75 mg kg^{-1} pentobarbital (Nembutal) by intraperitoneal injection and placed into CLAMS cages pre-acclimated to 33°C to maintain mouse body temperature while under anesthesia. Prior to norepinephrine induced oxygen consumption readings, baseline oxygen consumption measurements were recorded for several cycles following pentobarbital administration until stable readings were recorded. A subcutaneous injection of 1 mg kg^{-1} L-(−)-Norepinephrine (+)-bitartrate salt monohydrate (Sigma, A9512) dissolved in sterile 0.9% NaCl (Sigma, S8776) was performed into the dorsal nuchal region. Following injection, individual mice were immediately placed into the CLAMS cages and oxygen consumption rates were recorded until rates began to decline.

In vivo metabolic phenotyping

Whole-body energy metabolism was evaluated using a Comprehensive Lab Animal Monitoring System (CLAMS, Columbia Instruments). Mice were singly housed and acclimated metabolic chambers for 48 h prior to data collection. Each mouse was

continuously monitored for physical activity and food intake. CO_2/O_2 levels were collected 4–5 times per hour per mouse over the duration of the experiment. NMR Body composition analyses were performed using Echo-MRI (Echo Medical Systems) to measure fat and lean mass. ANCOVA analysis of VO_2 versus body mass during light, dark, and 24 h periods was performed through the NIDDK Mouse Metabolic Phenotyping Centers Energy Expenditure Analysis website (http://www.mmpc.org/shared/regression.aspx).

BAT Mitochondrial Respiration Assays

Mitochondrial respiration rates were determined using an O2K high-resolution respirometer (Oroboros Instruments, Austria). To preserve all populations of mitochondria, whole tissue homogenates were prepared from BAT minced on ice and dounced at 4°C (150 rpm X 8 strokes) in 15 ml of ice-cold mitochondrial isolation buffer (MIB, mannitol 210 mM, sucrose 70 mM, Hepes 10 mM, EGTA 1 mM, adjusted to pH 7.2 with KOH)[34,35,36]. Homogenates were centrifuged at 8,500 x g for 10 minutes at 4°C. Lipid and supernatant were discarded. Pellet was re-suspended in 1 ml of ice-cold MIB, passively filtered (100 μm), and protein concentration determined by BCA assay.

Respirometry measurements were performed using homogenates (0.25 mg) resuspended in respiration buffer and maintained at 37°C (110 mM mannitol, 0.5 mM, EGTA, 3 mM $MgCl_2$, 20 mM taurine 10 mM KH_2PO_4, 60 mM K lactobionate, 0.3 mM DTT, and 0.1% BSA (fatty acid free), adjusted to pH 7.1). Samples were vigorously stirred via magnetic stir bar and the O2 concentration maintained between 100 and 200 nmol/ml. UCP1-dependent respiration and individual complex dependent respiration rates were determined by a standard substrate/inhibitor titration protocol. Following stabilization, real-time oxygen concentration and flux data were collected continuously (DatLab software 4.3, Oroboros Instruments, Austria). Baseline respiration following the addition of substrate (palmatoylcarnitine (4 mM), pyruvate (10 mM) and malate (5 mM)) was measured. UCP1-dependent respiration was assessed by addition of 2 mM GDP. Independent complex dependent respiration was then determined in the presence of ADP (1 mM). To assess complex II (CII)-dependent respiration, rotenone (0.5 μM) was added to selectively inhibit CI followed by succinate (10 mM), a CII substrate. Antimycin A (5 μM) was then added to inhibit complex III (CIII) followed by addition of TMPD (0.5 mM) and ascorbate (2 mM) as artificial electron donors for complex IV (CIV). Sodium Azide (2.5 mM) was used to assess the contribution of leak respiration independent of CIV.[37,38]

Histologic analysis

Adipose tissues were fixed in 4% paraformaldehyde/1x PBS overnight at 4°C and dehydrated through sequential ethanol washes. Tissue was embedded in paraffin prior to sectioning and then stained with hematoxylin and eosin (H&E). Stained sections were visualized and photographed under bright-field microscopy.

RNA Isolation and Gene Expression Analysis (RT-qPCR)

Total RNA was isolated from snap-frozen adipose tissues, which were mechanically homogenized in 500ul TRIzol (Life Technologies) in a TissueLyser (Qiagen) for 5 minutes, at a frequency of 20 s^{-1}. Following homogenization, samples were centrifuged at 4°C and

homogenates transferred to a fresh tube for RNA extraction with chloroform. Aqueous chloroform fractions were mixed with equal volumes of 70% ethanol/30% water and RNA further purified with RNeasy Mini spin columns (Qiagen) and on-column DNase-digestion (Qiagen). TRIzol phases were saved for further isolation of genomic and mitochondrial DNA. 1.5 μg of total RNA was used for complementary DNA synthesis using a High-Capacity cDNA Reverse Transcription kit (Applied Biosystems). cDNAs were analyzed by qPCR using a Power SYBR Green PCR Master mix on the Quant Studio 6 Flex Real-Time PCR system (Applied Biosystems). All qPCR data were analyzed using a standard curve and normalized to *36B4 (Arbp)* or *18s* expression. Specific primer sequences are listed in primer table.

Quantification of Mitochondrial Content

Total DNA was precipitated from TRIzol tissue extraction by ethanol precipitation and centrifugation, followed by sodium citrate/ethanol solution (0.1 M sodium citrate/10% ethanol, pH 8.5) washes of DNA pellet. DNA pellet was allowed to air dry prior to re-suspension. DNA samples were analyzed by qPCR utilizing a standard curve to determine absolute mtDNA abundance normalized to nuclear genomic DNA abundance. Specific primer sequences are listed in primer table.

Immunoblotting

Interscapular BAT samples were homogenized in radioimmunoprecipitation assay (RIPA) buffer (150 mM NaCl, 1.0% NP-40, 0.5% Sodium-deoxycholate, 0.1% SDS, 50 mM Tris-HCl pH 8.0, 5 mM EDTA, 5 mM NaF, 1 mM Na_3VO_4) with 1 mM phenylmethylsulphonylflouride (PMSF), supplemented with complete protease inhibitor (Roche), using a TissueLyser (Qiagen) for 3 min a frequency at 20 s^{-1} at 4°C followed by sonication using a Biorupter (Diagenode) for 30 s. For nuclear extracts, nuclei were prepared by dounce homogenization of five frozen BAT pads thawed in swelling buffer plus protease inhibitor (10 mM Tris-HCl, 2 mM $MgCl_2$, 3 mM $CaCl_2$), dounced with pestle A/B, filtered with 100 μm cell strainer, and pelleted at 600 x g, re-suspended in swelling buffer and cells lysed in equal volume of lysis buffer (Swelling buffer + 10% glycerol + 1% NP-40). Nuclei were isolated by centrifugation at 600 x g and soluble protein extracted by re-suspending in 4 pellet volumes of modified nuclear extract buffer (20 mM HEPES, 0.42 M KCl, 3 mM $MgCl_2$, 10% glycerol, 3 mM 2-mercaptoethanol, 0.5% Trition-X, 1 mM EDTA, and 1 mM EGTA) plus protease inhibitors and incubated at 4°C with rotation for 2 hours. Protein concentration was determined using Direct Detect Spectrometer (EMD Millipore) and protein loaded onto 10% Criterion TGX gels (Bio-Rad) by SDS-PAGE, and transferred to a polyvinylidene difluoride (PVDF) membrane. After antibody incubation, immunoblots were visualized using enhanced chemiluminescence (ECL) substrates (Western Lightning Plus-ECL, PerkinElmer; or SuperSignal West Dura, Thermo) by autoradiography film or Bio-Rad ChemiDoc Imaging.

Antibodies

The following antibodies were used for western blotting: HDAC3 (GeneTex, GTX113303, Lot 40436), β–Actin [mAbcam 8226] (ABCAM, 20272), ERRα (ABCAM, 16363), HSP90 (Cell Signaling, 4874), Vinculin (Sigma, V9264), Acetylated Lysine Rabbit Polyclonal (Cell

Signaling, 9441, Lot 12), UCP1 (R&D, MAB6158), HA Tag (GeneTex, 115044-01), Myc Tag (GeneTex, 21261), V5 Tag (ThermoFisher, R960-25), Pol II Antibody (N-20, Santa Cruz 899 X, Lot K1215), GCN5 (H-75, Santa Cruz 20698, Lot K0112), PGC-1α Mouse mAb (EMD Millipore, 4C.13, ST1202, Lot TE0349482), Anti-Rabbit IgG-HRP (Cell Signaling, 7074), Anti-mouse IgG-HRP (Cell Signaling, 7076), Mouse monoclonal SB62a Anti-Rabbit IgG light chain (HRP) (ABCAM, 99697). The following antibodies were used for ChIP: HDAC3 (ABCAM, 7030, Lot GR121157-6), H3K27ac (ABCAM, 4729, Lot GR251958-1), ERRα (ABCAM, 16363, Lot GR263385-1), NCoR (previously described[39], raised in rabbit against a.a.1944–2453, affinity purified), H3K4me1 (ABCAM 8895), and H3 (ABCAM 1791).

Cell Culture

NIH/3T3 cells (ATCC, CRL1658) were maintained at 37°C in 5% CO2 in high glucose Dulbecco's modified Eagle's medium (DMEM) supplemented with 10% Bovine Calf Serum (Sigma) and 1% Penn/Strep (Gibco). 293FT cells (Thermo, R700-07) were maintained at 37°C in 5% CO2 in high glucose Dulbecco's modified Eagle's medium (DMEM) supplemented with 10% Fetal Bovine Serum (Tissue Culture Biologicals) and 1% Penn/Strep (Gibco). All lines were passaged at ~80–85% confluence. Immortalized brown pre-adipocytes[40] were maintained at 37°C in 5% CO2 in DMEM/F-12 Glutamax, 10% FBS, 1% Penn/Strep (Gibco). NIH/3T3 and 293FT cell lines were low passage and not tested for mycoplasma. Immortalized brown pre-adipocytes tested negative for mycoplasma using the MycoAlert Mycoplasma Detection Kit (Lonza).

Primary Brown Adipocyte Isolation and Differentiation

Matings of *Rosa26*-CreER-positive, HDAC3$^{F/F}$ x HDAC3$^{F/F}$ mice were used to generate *Rosa26*-CreER-postive, HDAC3$^{F/F}$ and littermate control HDAC3$^{F/F}$ pups. Pre-adipocytes were isolated from BAT depots of postnatal day 1–3 mice and tails saved for genotyping. Individual depots were placed into 200μl DMEM/F-12 Glutamax (Invitrogen) and minced finely with spring scissors (Roboz) prior to digestion in 1 ml 1.5 U ml^{-1} collagenase D (Roche) and 2.4 U ml^{-1} Dispase II (Roche) at 37°C in thermocycler for 40 minutes at 1200 rpm. Cells were purified through 100μm filters (Millipore) into 5ml of DMEM/F-12 Glutamax with 10% FBS, pelleted at 700 x g, and re-suspended in growth media (DMEM/F-12 Glutamax, 10% FBS, 1% Penn/Strep (Gibco), and primocin (Invivogen)). Pre-adipocytes of the same genotype were pooled, re-plated and upon confluence, adipocyte differentiation was initiated with induction media (growth media supplemented with 500 nM dexamethasone, 125 μM indomethacin, 0.5 mM IBMX, 1 μM Rosi, 1 nM T3, 20 nM insulin) for 48h. Following induction, cells were cultured in maintenance media (Growth media plus 1 nM T3, 20 nM insulin) and media refreshed every 48 h. For inducible HDAC3 deletion experiments, 2 μM 4-hydroxytamixofen (4-OHT, Sigma) was added to induction media of both *Rosa26*-CreER-positive and *Rosa26*-CreER-negative cells from Days 0–2. All analysis was carried out on Day 8 cultured brown adipocytes.

Retrovirus

Wild-type *Pgc-1α* and a non-acetylatable *Pgc-1α* mutant (R13) cDNAs were cloned into an MSCV retroviral construct. Retrovirus was produced in HEK-293FT cells by co-transfection

of MSCV and pCL-Eco vectors with FuGENE 6 (Promega), and supernatants were harvested 72 h post-transfection. Supernatants were passed through a 0.20μm filter (Corning) prior to viral concentration with PEG-it Virus Precipitation Solution (System Biosciences) at 4°C. 24 well plates were seeded with 6×10^4 brown pre-adipocytes per well and MSCV retroviruses were added upon cell adherence in media containing 2 μg mL^{-1} polybrene and allowed to reach confluence prior to adipocyte differentiation.

Dual Luciferase Assays

The mouse *Ucp1* (−6k) enhancer (389 bp) containing ERRα and HDAC3 binding sites, was PCR-amplified from C57BL/6 genomic DNA using primers listed in primer table to add XhoI and BglII sites for cloning into the pGL4.24 luciferase vector (Promega). The mouse *Pgc-1α* (−38k) enhancer (998bp) containing identified binding sites, was PCR-amplified from C57BL/6 genomic DNA using primers listed in Supplemental Table 1 and Gibson cloned between the NheI and BglII sites of the pGL4.24 luciferase vector. Luciferase assays were performed by transient transfection of NIH/3T3 cells seeded at a density of 1.25×10^5 cells per well (24-well plate) using Lipofectamine 2000 (3:1 ratio, Lipofectamine:DNA). Optimized transfections were performed using 1,200ng DNA: 500ng pGL4.24 luciferase vector and 2.0ng Renilla (for normalization) plus factor expression vectors and/or empty pcDNA3.1. 24 hours after transfection, cell lysates were harvested using the Dual Luciferase Kit (Promega) to measure luciferase activities on a Synergy HT plate reader (Biotek).

Immunoprecipitation Assays

For cellular acetylation experiments, 293FT cells were co-transfected with combinations of pcDNA3.1-GFP, pcDNA3.1-HA-PGC-1α, pcDNA3.1-HDAC3-myc, pcDNA3.1-Flag-GCN5, and/or empty pcDNA3.1. 48 h after transfection, cells were harvested in ice-cold NP40 IP Lysis Buffer (20 mM Tris-HCl, 150 mM NaCl, 10% glycerol, 2 mM EDTA, 0.1% NP40, 10 mM NaF, with 1 mM DTT, 1 mM phenylmethylsulphonylflouride (PMSF), and supplemented with complete protease inhibitor cocktail (Roche), 4 μM Trichostatin A (TSA, Cell Signaling), 5 mM nicotinamide (Sigma), and 1 μM Bortezomib (Cell Signaling) on ice. Cell lysates were freeze/thawed in liquid nitrogen twice, and lysates cleared by centrifugation at 4°C for 10 minutes. 250 mg of protein was used for each immunoprecipitation and volume adjusted to 1ml with lysis buffer. Washed anti-HA Agarose beads (Pierce) were incubated with samples and rotation at 4°C for 4 h, followed by three brief washes with lysis buffer. Immunoprecipitated proteins were eluted in 2X loading buffer with boiling at 95°C for 5 minutes.

Co-immunoprecipitation

For endogenous co-immunoprecipitations, protein lysates were made from Day 8 differentiated brown adipocytes in IPLS buffer (50 mM Tris-HCl pH7.4, 150 mM NaCl, 0.5% NP-40) with protease and phosphatase inhibitor (Roche). Lysates were sonicated, lipid removed by centrifugation at 4°C, and 0.5 mg protein lysate was pre-cleared with anti-rabbit Trueblot beads (Rockland) for 3 hours at 4°C with rotation. 1% of total pre-cleared lysate was saved for input. Pre-cleared lysate was then incubated with anti-HDAC3 (Abcam, 7030) at 4°C for 2 h with rotation, followed by immunoprecipitation with conjugated anti-rabbit goat IgG Trueblot beads for 1 h at 4°C. Beads were washed four times with IPLS buffer plus

inhibitors and samples eluted in 2x loading buffer at 55°C for 20 min with agitation, supernatant isolated from beads, BME and DTT added, and boiled at 95°C for 5 min. Eluted proteins were resolved by immunoblotting and PVDF membrane incubated with anti-ERRα (Abcam, 16363) overnight at 4°C, a conformation specific secondary mouse anti-rabbit IgG–HRP, and then developed. The blot was stripped (Restore Plus, Thermo), blocked, and incubated overnight at 4°C with HDAC3 (Abcam, 76295) followed by incubation with conformation specific secondary mouse anti-rabbit-HRP. For overexpression co-immunoprecipitation experiments V5-tagged ERRα, and/or HA-tagged PGC-1α and myc-tagged HDAC3 were co-transfected into HEK-293FT cells for 48 h. 48 h after transfection, cells were harvested in ice-cold IPLS Buffer supplemented with complete protease inhibitor cocktail, 1 mM PMSF, 1 μM Bortezomib on ice. Cell lysates were freeze/thawed in liquid nitrogen twice, sonicated, and lysates cleared by centrifugation at 4°C for 10 minutes. 100 mg of lysate was pre-cleared with Mouse IgG Sepharose bead conjugate (Cell Signaling, 3420) prior to immunoprecipitation with V5-agarose beads (Sigma, A7345) at 4°C for 2 h. Beads were washed four times in IPLS Buffer and eluted in 2X loading buffer at 95°C for 5 min, supernatant isolated from beads, BME added and boiled at 95°C for 5 min. Immunoblot for myc-HDAC3 was performed using goat anti-myc HRP (GeneTex), stripped, re-developed, and then immunoblotted for V5-ERRα with mouse monoclonal anti-V5 (ThermoFisher).

Protein purification

HA-tagged PGC-1α was co-transfected into HEK-293FT cells with GCN5 for 48 h and the cells were lysed in RIPA lysis buffer supplemented with complete protease inhibitor cocktail (Roche), 1 mM phenylmethylsulphonylflouride (PMSF), 4 μM TSA (Cell Signaling), 5 mM nicotinamide, and 1 μM Bortezomib (Cell Signaling) on ice. Lysate was sonicated, cleared by centrifugation, and immunoprecipitation of acetylated PGC-1α performed with anti-HA agarose beads (Pierce) performed at 4°C with rotation in the presence of inhibitors. Sequential washes (with inhibitors) were performed: six washes with RIPA buffer, two washes high salt wash buffer (10 mM Tris-HCl pH 8.0, 250 mM LiCl, 0.5% NP-40, 0.5% Sodium-deoxycholate, 1 mM EDTA), followed by two washes in 1x PBS. The purified protein remained immobilized on HA-beads in the presence of inhibitors prior to de-acetylation assay.

In vitro de-acetylation assay

Immobilized pre-acetylated PGC-1α was washed three times with HDAC assay buffer (Enzo). 30μl of the bead slurry was added to 100μl HDAC assay buffer containing buffer alone, 100ng recombinant human HDAC3/NCoR-DAD (Enzo), or 100ng recombinant human HDAC3/NCoR-DAD plus 4μM TSA, and incubated at 37°C with agitation for 1 h. After the reaction, the beads were boiled in 2X loading buffer with BME at 95°C and acetylation of PGC-1α was assessed by western blot.

Acute siRNA knockdown in immortalized brown adipocytes

Acute siRNA knockdown was performed via reverse-transfection. 6×10^4 differentiated brown adipocytes (Day 5) were seeded into 96-well plates containing Lipofectamine RNAiMax and siRNAs (pre-incubated for 25 minutes in wells) or into no transfection

control. Total RNAi concentration was held constant at 50nM. 72 hours post-transfection, Day 8 brown adipocytes were harvested in Trizol for analysis by RT-qPCR. ON-Target Plus SMARTpool siRNAs targeting mouse *ERRα* (Dharmacon, L-040772-00, Target sequence: 5′-GCUGAAAGCUCUGGCCCUU-3′, 5′-GCGGAGGACGGCAGAAGUA-3′, 5′-CUGAGAAGCUGUACGCCAU-3′, 5′-GCAUCGAGCCUCUCUACAU-3′), *Ppargc1α* (Dharmacon, L-040773-01, 5′-GAACAAGACUAUUGAGCGA, 5′-UUACGCAGGUCGAACGAAA-3′, 5′-ACAAUGAGCCUGCGAACAU-3′, 5′-CAGCCGAGGACACGAGGAA-3′), *Ppargc1β* (Dharmacon, L-040905-01, 5′-UGGUACAGCUCAUUCGCUA-3′, 5′-GGGAAAAGCAAGUACGAAG-3′, 5′-GCUUUGAGGUGUUCGGUGA-3′, 5′-GGAAAAGGCCAUCGGUGAA-3′) or *non-targeting control* (Dharmacon, D-001810-10, 5′-UGGUUUACAUGUCGACUAA-3′, 5′-UGGUUUACAUGUUGUGUGA-3′, 5′-UGGUUUACAUGUUUUCUGA-3′, 5′-UGGUUUACAUGUUUUCCUA-3′) were used.

RNA-seq library preparation

Total RNA was extracted from interscapular BAT pads of 12-week old male mice adapted to thermoneutrality for two weeks. 1.0 μg of purified DNase-treated total RNA from biological replicates (4 wild-type control HDAC3$^{F/F}$, 4 knockout *Adipoq*-Cre; HDAC3$^{F/F}$) were processed with the Ribo-Zero Magnetic rRNA removal kit (Epicentre, MRZH11124). The RNA libraries were prepared using the TruSeq RNA Sample Prep Kit v2 (Illumina, RS-122-2001) and standard Illumina protocol. RNA-seq libraries were sequenced at single-end 100bp read length on an Illumina HiSeq 2000.

RNA-seq data analysis

RNA-seq reads were aligned to the UCSC mm9 using Tophat2[41]. For differential gene expression analysis, raw read counts were measured within RefSeq genes using feature Counts[42], and an exact test was performed using the edgeR pipeline[43]. Genes were included in differential expression analysis if their expression levels were > 0.5RPKM in at least three samples. Genes having a fold-change > 1.5 (either up or down) and FDR < 0.01 were selected as HDAC3-KO-regulated genes. Gene ontology (GO) analysis was performed using Enrichr[44,45], where the top ranked KEGG pathway, Biological Process and Cell Component terms were selected by Enrichr combined score. Representative down-regulated genes identified by gene ontology were presented with their log2FC as a heatmap. As an extended figure, all TCA cycle and mitochondrial respiratory chain complex genes retrieved from the HUGO gene nomenclature database[46] were presented by heatmap to show quantitative trend identified in GO. For genome browser visualization, bigwig files[47] were generated for individual replicates in a 1bp-resolution RPM scale using genomeCoverageBed with ‘-split’ option in bedtools[48] and bedGraphToBigWig in SRA toolkit[49]. A representative track was generated for each condition from the replicate bigwig files. All the genome browser snapshots were taken via IGV[50,51].

Chromatin-immunoprecipitation

HDAC3 ChIP was performed as previously described[39,14] with modification. Immediately following euthanasia, the entire interscapular BAT pad (2 lobes) was snap-frozen. Tissue was later thawed and minced directly in cross-linking solution (10mls, 1x PBS/1%

formaldehyde) and allowed to rock for 20 minutes at room temperature. For epididymal white adipose tissue (eWAT) ChIP, 2 fat pads per were processed in an identical fashion to BAT. Cross-linking was quenched by addition of 0.5 mL of 2.5 M glycine and allowed to mix for 5 minutes, followed by three ice-cold 1x PBS washes. Cross-linked tissue pieces were re-suspended in ice-cold ChIP Dilution buffer (50 mM HEPES pH7.5, 155 mM NaCl, 1 mM EDTA, 1.1% Triton X-100, 0.11% Sodium-deoxycholate, 0.1% SDS) with protease inhibitors (Complete Protease inhibitor, Roche) and placed on ice. Chromatin fragmentation was performed using probe sonication at 4°C (Fischer Scientific, FB705 Sonic Dismembrator) for three cycles of 10 seconds at 10% amplitude, followed by three cycles of 10 seconds at 15% amplitude, with a 30 second pause on ice between cycles. Chromatin lysates were cleared of lipid by centrifugation at 4°C. Chromatin lysates were brought to 1 ml with ChIP dilution buffer, input saved, and incubated with antibodies overnight at 4°C, then immunoprecipitated with BSA blocked Protein A Sepharose CL-4B Beads (GE healthcare) with rotation for 2 h at 4°C. Immunoprecipitations were washed: one quick wash 1 ml ChIP Dilution Buffer, one 5 minute wash ChIP Dilution Buffer, one 5 minute wash in 1 ml ChIP Dilution Buffer with 500 mM NaCl, one 5 minute wash in ChIP Wash Buffer (10 mM Tris-HCl pH 8.0, 250 mM LiCl, 0.5% NP-40, 0.5% Sodium-deoxycholate, 1 mM EDTA), followed by one five minute wash in Tris-EDTA (10 mM Tris-HCl pH 8.0, 1 mM EDTA). Cross-linking was reversed overnight at 65°C in elution buffer (50 mM Tris-HCl pH 8.0, 10 mM EDTA, 1% SDS), removed from beads, incubated with proteinase K, and DNA was isolated using phenol/chloroform extraction in 2 ml Phase Lock Gel tubes (5 Prime) followed by NaCl/EtOH mediated DNA precipitation overnight at −20°C with 20 μg glycogen carrier (Roche).

ChIP-seq library preparation

For BAT ChIP-seq of HDAC3, ERRα, and NCoR, 5 biological replicate ChIPs were pooled for sequencing. For BAT ChIP-seq of H3K27ac, replicate ChIPs were pooled into 2 libraries (3 samples per library) for sequencing and library reads pooled into one data set. Enzymes from New England Biolabs were used to generate libraries according to the ChIP Sequencing Sample Preparation Guide provided by Illumina. Adaptor oligos and primer sequences from Illumina were utilized for library construction and amplification. Prior to PCR library amplification, size selection of adaptor ligated DNA was performed using Agencourt AMPure XP Beads (Beckman Coulter). PCR Purification and MinElute (QIAGEN) kits were used for library purification steps.

ChIP-seq data analysis

All ChIP-seq libraries were sequenced on HiSeq 2500 (single-end 50bp or 100bp) or NextSeq 500 (single-end 75bp or 76bp). Before alignment, all reads were adjusted to 50bp by trimming 3′-end to avoid any bias due to different read lengths. Sequencing reads were aligned to the UCSC mm9 using Bowtie[52]. All peak calling was performed using the findPeaks command in Homer package[53]. For HDAC3 peak calling, WT and HDAC3-KO aligned reads were down-sampled to 20 million reads to adjust read-depth bias and avoid peak saturation, and duplicate reads were removed except for one. Stringent HDAC3 peaks were called in the WT sample against the KO sample using option ‘-F 3’ (FDR < 0.001). ERRα peaks in WT and HDAC3-KO mice and NCoR peaks in WT mice were called against

an input using default options (FDR < 0.001). After initial peak calling, all peaks were resized into 200bp followed by 1 RPM cutoff and peaks within the ENCODE blacklist regions[54] were discarded. When visualizing HDAC3, ERRα. NCoR ChIP-seq profile (line plots and heat maps), we used control-subtracted signal: KO sample for HDAC3, input sample for ERRα and NCoR. All bigwig files were generated using Homer and the bedGraphToBigWig command. HDAC3 and ERRa ChIP-seq signal were compared by RPM-normalized tag counts between KO-repressed and unchanged eRNAs within 400bp window, where *P*-value was calculated by Wilcoxon test.

Two biological replicates of H3K27ac ChIP-seq were prepared from both WT and HDAC3-KO BAT. Duplicate reads were condensed and replicates were pooled for visualization in a genome browser. H3K27ac levels at HDAC3-bound enhancer nearby KO-regulated genes were compared between WT and KO mice by RPM-normalized tag counts within 2kb window around HDAC3 peaks, and *P*-values were calculated by Wilcoxon test. Super-enhancers were called based on the H3K27ac data using a ROSE pipeline using default options. H3K4me1 and H3 ChIP-seq data in WT BAT and WT eWAT were generated to prepare an eRNA filter for GRO-seq analysis. Together with previously published adipose H3K27ac data[55] (GSE63964), histone modification peaks were called against corresponding H3 ChIP-seq sample in each depot by Homer with an option '-style histone -F 3' (FDR < 0.001).

De novo motif search within of ChIP-seq peaks were performed using the findMotifsGenome command in Homer within a 200bp window with default options. Discovered motifs were ranked by p-values calculated based on a binomial test against GC %-matched background, and the top four motifs presented.

GRO-seq library preparation

GRO-seq was performed and analyzed as previously described[22], with minor modifications for mouse interscapular BAT samples. 10 interscapular BAT pads from genotype confirmed *Adipoq*-Cre, HDAC3 KO and control littermates were quickly dissected, immediately pooled and minced in ice-cold nuclei isolation buffer A, and dounce homogenized on ice to isolate ~40 million nuclei. Aliquots of nuclei preparations were inspected visually for quality under a microscope with DAPI staining, and nuclei counted using a Countess Automated Cell Counter (Invitrogen). The nuclear run-on reaction was performed for 7 minutes and RNA hydrolysis was allowed to proceed for 10 minutes. All GRO-seq library preparations were performed in parallel to avoid batch effects.

GRO-seq data analysis

Prior to alignment, sequencing reads were cleaned by trimming off low quality base, adapter and poly-A tailing sequences using cutadapt[56]. Trimmed reads of at least 25bp were selected and aligned to UCSC mm9 using bowtie with an option '--best --strata -m 1 -v 3'. Aligned reads within extremely high signal regions (such as rRNA, snoRNA, snRNA and tRNA) were removed before downstream analysis to minimize read-depth bias. For genome browser visualization, bigwig files were generated separately for (+) and (−) strands, and all

reads were extended to 150bp for smooth profile. All (−) strand signals were presented as negative values.

Gene body transcription levels were quantitated in all conditions for comparative analysis. First, all reads were extended to 50bp toward the 3′-end, then RPKM-normalized read counts were measured within RefSeq gene bodies excluding the 500bp region at the 5′-end. However, for genes with total gene length < 1kb, the entire gene body was used. Gene transcription levels were further normalized among conditions for global bias correction using loess normalization in limma package[57]. A gene was classified as 'transcribed' in a given condition if the transcription level was > 0.3 RPKM. Genes that were not transcribed throughout all conditions were eliminated before downstream analysis. A gene was defined as 'differential' between a given pair of conditions if it was transcribed in either condition and the fold-change was greater than 1.5 (either up or down). *Ucp1* and *Ppargc1α* nascent transcription levels were compared between genotypes and between temperatures via an exact test in EdgeR[43,58] using a common dispersion estimated from housekeeping genes.

Hierarchical clustering was performed for nascent gene transcription level at 22°C and 29°C in WT and HDAC3 KO mice to identify an HDAC3-dependent functional module. First, putatively highly variable genes were selected by fold change > 1.5 between maximum and minimum transcription level. Next, clustering was done for $\log_2$-transformed gene transcription level by Ward's criterion using Pearson correlation coefficient as a similarity measure. One cluster of genes was identified that display similar transcriptional changes to *Ucp1* or *Ppargc1α* genes. Overall gene transcription trend was visualized as a boxplot in z-score scale. Next, gene ontology analysis was performed for this cluster using Enrichr; top ranked Biological Process term and KEGG pathway were selected and their relative gene transcription levels were visualized by a heatmap in z-score scale.

eRNA calling was performed as previously described[22,59] with minor optimization. First, eRNA peaks were called separately on each strand for all samples via Homer peak calling using option '-style factor -separate -center -fragLength 150 -size 200 -minDist 400 -tbp 0 -L 3 -localSize 10000 -fdr 0.001'. Next, another round of peak calling was performed using the same option for intergenic reads only to rescue promoter-proximal eRNA peaks skipped by local background effect of highly transcribed genes. All eRNA peaks, excluding ones falling into TSS 2kb and TTS 2kb windows, were then pooled and merged among biological conditions to prepare a master eRNA peak sets. Next, a series of filters were applied: 1) peaks within ENCODE blacklist regions were discarded; 2) small peaks (< 0.2RPM) or any peaks embedded within same-stranded gene transcription were discarded; 3) an epigenomic filter was applied using active enhancer marks, H3K27ac and H3K4me1 from BAT and eWAT, to broadly define and capture adipose eRNAs. Remaining peaks were then paired between opposite strands if their distance was < 1kb. For paired eRNA peaks, their center was defined as an enhancer; for unpaired eRNA peaks, their 5′ upstream 180bp positions were defined as enhancers.

eRNA transcription levels were measured in RPKM within a 1kb window around enhancers. If an enhancer was intergenic, both strands were measured; if it was within a transcribed gene body, only anti-sense signal was measured. After measuring eRNA levels in all

conditions, loess normalization was applied for global bias correction as was previously performed in the gene transcription analysis. For differential analysis comparing two different conditions, eRNAs with > 0.5 RPKM in at least one condition were selected, then eRNAs with a fold-change > 2 (either up or down) were defined as differential eRNAs. *De novo* motif search for eRNAs was performed within 400bp window using Homer, and the top four motifs selected by p-value were presented.

Data availability

All ChIP-seq, RNA-seq, and GRO-seq data reported here have been deposited in GEO under accession number GSE83928. Source data and uncropped gels for figures provided with the paper. Data that support the findings of this study are available from the corresponding author upon request.

Extended Data

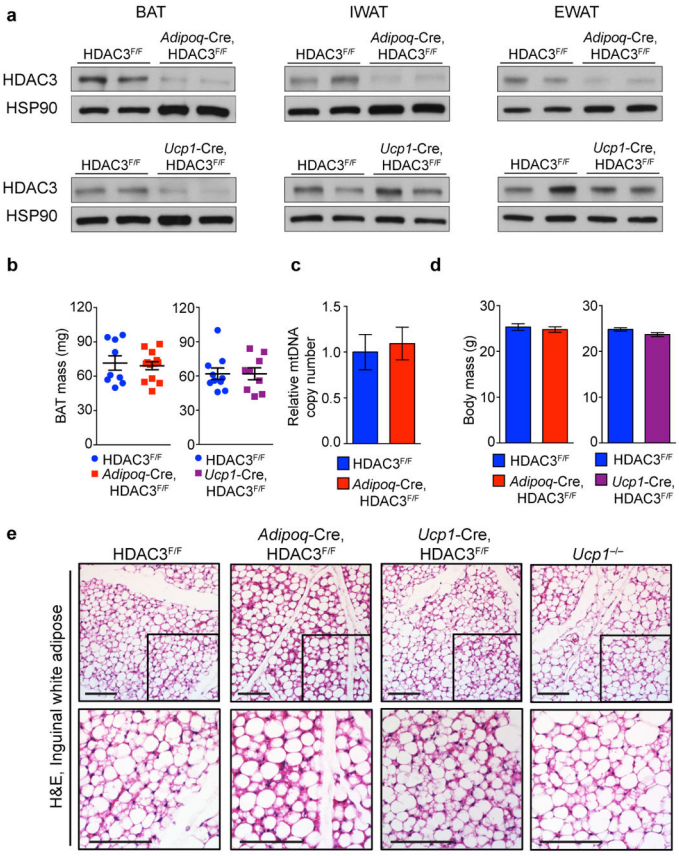

Extended Data Figure 1. Ablation of HDAC3 in adipose tissue depots

(a) Immunoblot analysis of interscapular BAT, inguinal WAT, and epididymal WAT of *Adipoq*-Cre HDAC3 KO and control littermates, or *Ucp1*-Cre HDAC3 KO and control littermates maintained at 22°C (n= 2, all groups) demonstrating tissue-specific conditional knockout of HDAC3. **(b)** Interscapular BAT mass, **(c)** Relative BAT mitochondrial number, and **(d)** Total body mass from *Adipoq*-Cre HDAC3 KO and *Ucp1*-Cre HDAC3 KO versus

control littermates maintained at 22°C (n= 13 *Adipoq*-Cre, n= 9 control; n= 9 *Ucp1*-Cre, n= 10 control). **(e)** Representative hematoxylin and eosin (H&E) staining of inguinal white adipose from 10–12 week old *Adipoq*-Cre HDAC3 KO, *Ucp1*-Cre HDAC3 KO, *Ucp1* KO, or control mice housed at 22°C. Scale bars, 100μm. Data are represented as mean ± s.e.m.

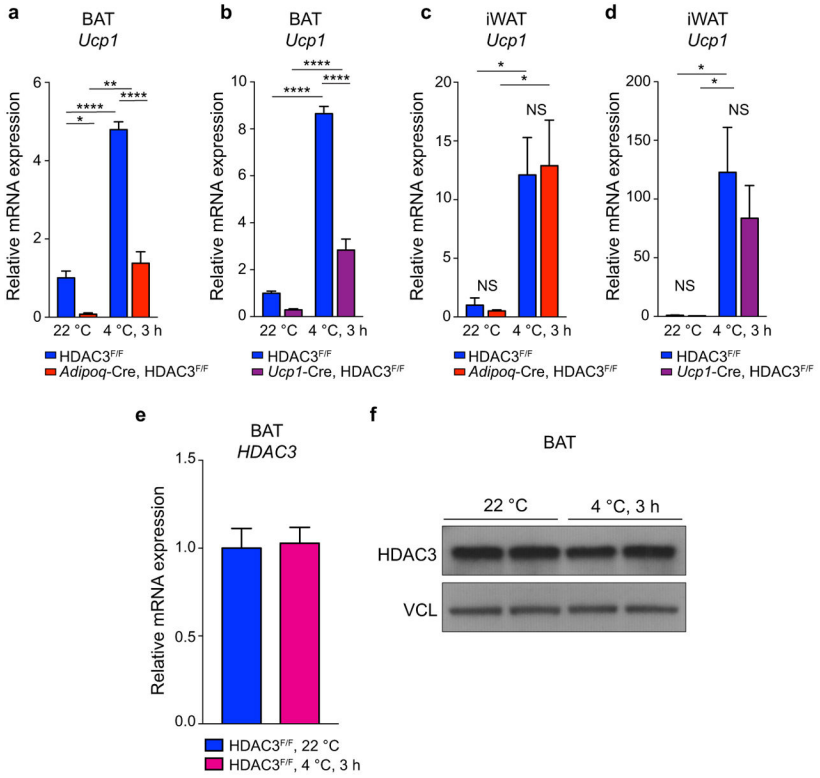

Extended Data Figure 2. BAT HDAC3 is required for cold-mediated induction of *Ucp1* expression and HDAC3 expression is not altered by acute cold

a–b BAT *Ucp1* mRNA levels following a 3 h exposure to 4°C (from 22°C) versus control littermates maintained at 22°C in **(a)** *Adipoq*-Cre HDAC3 KO versus control (n= 5, 5, per temperature) and **(b)** *Ucp1*-Cre HDAC3 KO versus control (n= 5, 5, per temperature). **c–d** iWAT *Ucp1* mRNA levels following 3 h exposure to 4°C, versus control littermates maintained at 22°C in **(c)** *Adipoq*-Cre HDAC3 KO versus control (n= 5, 5, per temperature) and **(d)** *Ucp1*-Cre HDAC3 KO versus control (n= 5, 5, per temperature). **(e)** BAT *HDAC3* mRNA expression levels following a 3 h exposure to 4°C (from 22°C) versus control littermates maintained at 22°C (n= 5, 5, per temperature). **(f)** BAT HDAC3 protein levels following 3 h acute cold exposure at 4°C (from 22°C) versus control littermates maintained at 22°C. VCL, vinculin. NS, not significant, *P<0.05, **P<0.01, ***P<0.001, ****P<0.0001 as determined by a two-way ANOVA and Holm-Sidak's post-test (a–d) or two-tailed Student's t-test (e). Data are represented as mean ± s.e.m.

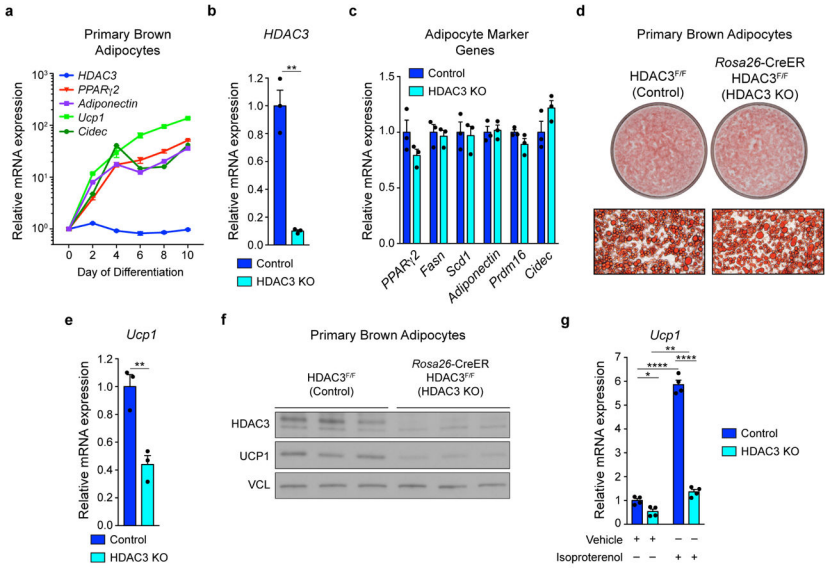

Extended Data Figure 3. HDAC3 is neither induced nor required for brown adipogenesis, but required for cell-autonomous *Ucp1* expression

(a) Gene expression spanning differentiation of cultured wild type primary brown adipocytes (n= 5 replicates per time point). **(b)** Depletion of HDAC3 in Day 8 cultured mature brown adipocytes following addition of 2μm 4-hydroxytamixofen (4-OHT) during Days 0–2 of differentiation to *Rosa26*-CreER-positive (HDAC3 KO) and *Rosa26*-CreER-negative (Control) cells derived from littermates (n= 3, 3). **(c)** Adipocyte-specific gene expression in cultured primary brown adipocytes following depletion of HDAC3 versus control (n= 3, 3). **(d)** Assessment of lipid accumulation (evaluated by Oil Red-O staining) in cultured HDAC3 KO versus control primary brown adipocytes. **(e)** *Ucp1* mRNA expression in cultured primary brown adipocytes following depletion of HDAC3 versus control (n= 3, 3). **(f)** UCP1 protein expression in cultured primary brown adipocytes following depletion of HDAC3 versus control. (n= 3, 3). **(g)** *Ucp1* mRNA expression in cultured primary brown adipocytes following depletion of HDAC3 versus control and treated with vehicle (ethanol) or isoproterenol (1μm) for 3 h (n= 4 per group). VCL, vinculin. **P*<0.05, ***P*<0.01, ****P*<0.001, *****P*<0.0001, as determined by a two-tailed Student's *t*-test (b, c, e) or by a two-way ANOVA and Holm-Sidak's post-test (g). Data are represented as mean ± s.e.m.

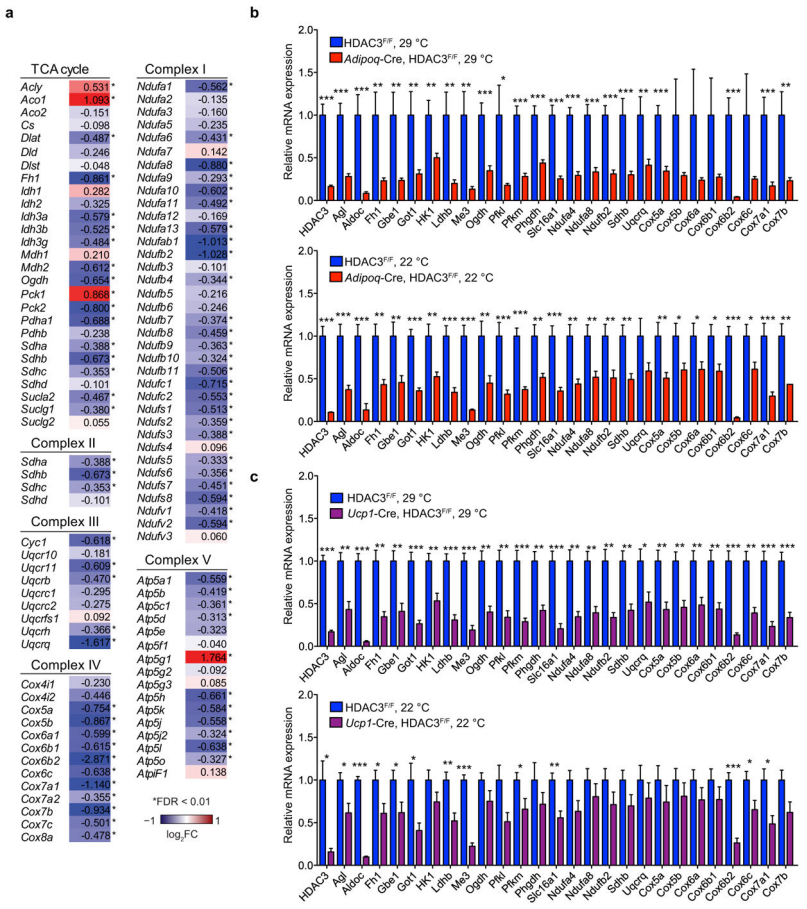

Extended Data Figure 4. HDAC3 is required for expression of mitochondrial OXPHOS and TCA cycle genes

(a) Bioinformatic extension of identified Gene Ontology categories (Fig 2c.) to all oxidative phosphorylation and TCA cycle genes as retrieved by HUGO gene nomenclature database. Asterisk designates gene expression change in RNA-seq dataset with an FDR <0.01. **b–c,** RT-qPCR verification of gene expression changes highlighted in Figure 2d, in **(b)** *Adipoq*-Cre HDAC3 KO vs. control littermates at 29°C (*upper,* n= 9, 6) and 22°C (*lower*, n= 9, 7) **(c)** *Ucp1*-Cre HDAC3 KO vs. control littermates at 29°C (*upper,* n= 5, 6) and 22°C (*lower*, n= 5, 7). **P*<0.05, ***P*<0.01, ****P*<0.001, as determined by a two-tailed Student's *t*-test. Data are represented as mean ± s.e.m.

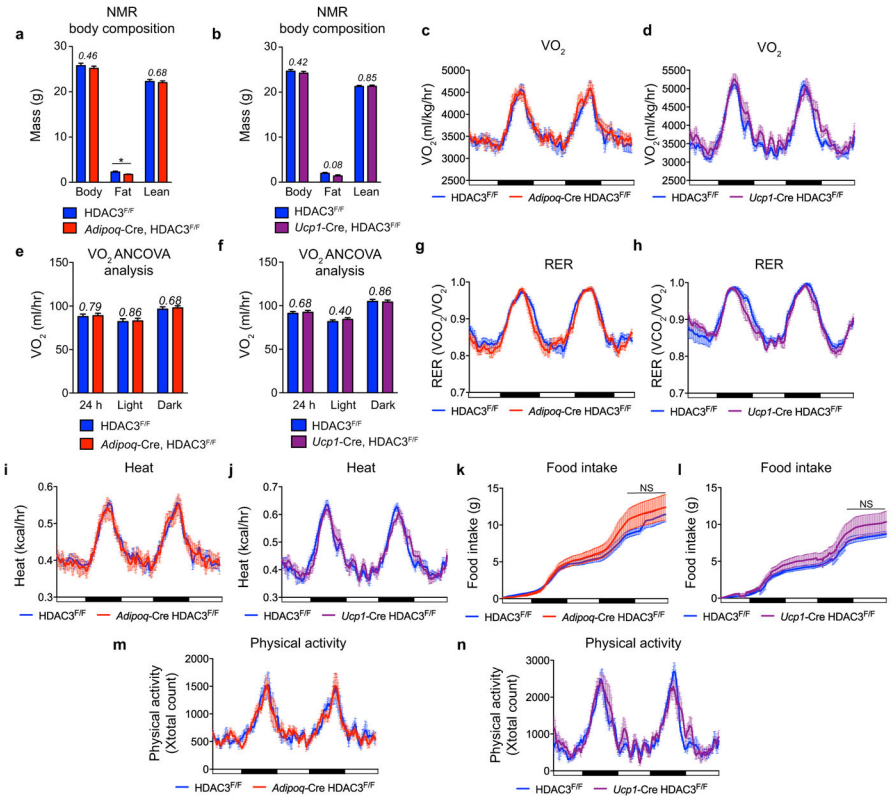

Extended Data Figure 5. Metabolic studies of *Adiponectin*-Cre and *Ucp1*-Cre HDAC3 KO mouse models

a–b NMR analysis of body composition, **(a)** *Adipoq*-Cre mice versus control littermates (n= 8, 11)**, (b)** *Ucp1*-Cre mice versus control littermates (n= 7, 9). **c–n**, CLAMS metabolic cage analysis. **c–d** Oxygen consumption (VO_2), **(c)** *Adipoq*-Cre HDAC3 KO vs. control littermates (n= 6, 5), **(d)** *Ucp1*-Cre HDAC3 KO vs. control littermates (n= 6, 6). **e–f** ANCOVA VO_2 analysis (linear regression analysis of total body mass and oxygen consumption) **(e)** *Adipoq*-Cre HDAC3 KO vs. control littermates (n= 6, 5)**, (f)** *Ucp1*-Cre HDAC3 KO vs. control littermates (n= 6, 6). **g–h** Respiratory Exchange Ratio (RER), **(g)** *Adipoq*-Cre HDAC3 KO vs. control littermates (n= 6, 5), **(h)** *Ucp1*-Cre HDAC3 KO vs. control littermates (n= 6, 6). **i–j** Heat measurements (kcal/hr), **(i)** *Adipoq*-Cre HDAC3 KO vs. control littermates (n= 6, 5). **(j)** *Ucp1*-Cre HDAC3 KO vs. control littermates (n= 6, 6). **k–l** Food Intake, **(k)** *Adipoq*-Cre HDAC3 KO vs. control littermates (n= 6, 5), **(l)** *Ucp1*-Cre HDAC3 KO vs. control littermates (n= 6, 6). **m–n** Physical activity, **(m)** *Adipoq*-Cre HDAC3 KO vs. control littermates (n= 6, 5), **(n)** *Ucp1*-Cre HDAC3 KO vs. control littermates (n= 6, 6). *P*-values shown in italics. CLAMS data is graphed as rolling averages. NS, not significant, **P*<0.05 as determined by a two-tailed Student's *t*-test (a–d, g–n) or ANCOVA (e, f). Data are represented as mean ± s.e.m.

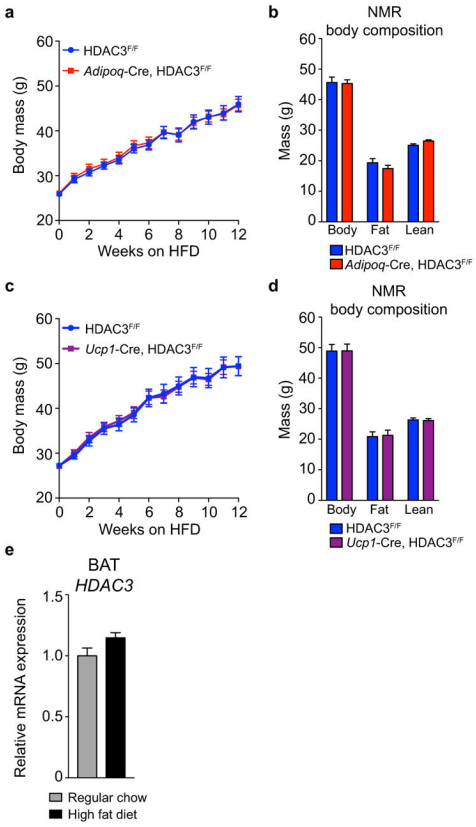

Extended Data Figure 6. Effect of high fat diet on *Adiponectin*-Cre and *Ucp1*-Cre HDAC3 KO mouse models

12-week old weight-matched HDAC3 KO and control littermates were fed high-fat diet (HFD) for 12 weeks (**a**) Weekly body weights, (n= 8 *Adipoq*-Cre, n= 10 control), (**b**) Body composition analysis by NMR, (n= 8 *Adipoq*-Cre, n= 10 control), (**c**) Weekly body weights, (n= 7 *Ucp1*-Cre, n= 7 control), (**d**) Body composition analysis by NMR, (n= 7 *Ucp1*-Cre, n= 7 control). **(e)** RT-qPCR of BAT *HDAC3* mRNA expression following 12 weeks HFD versus regular chow fed controls (n= 7, 5, respectively). Data are represented as mean ± s.e.m.

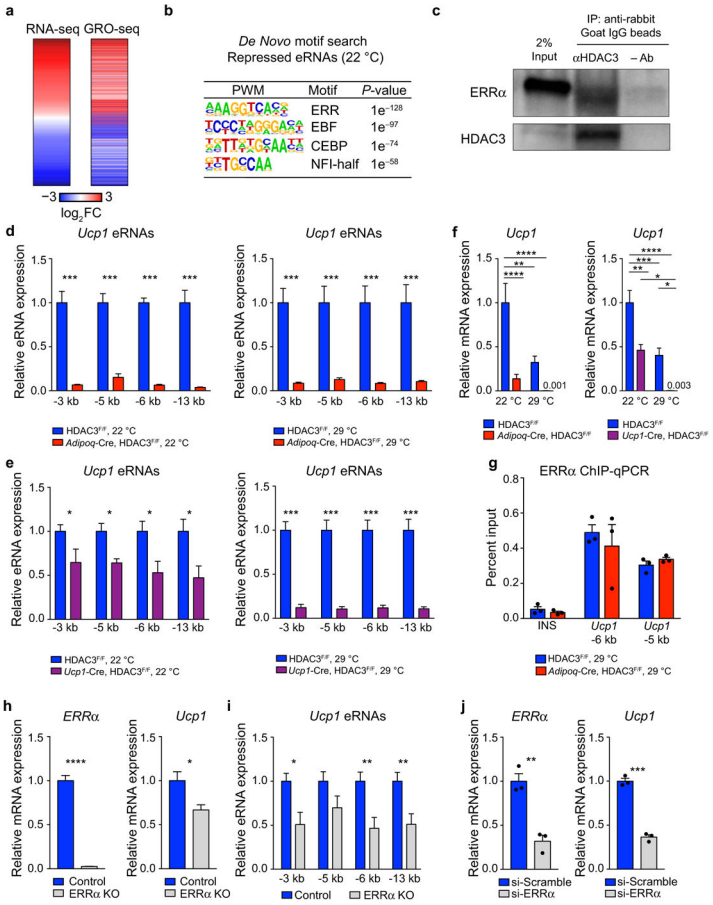

Extended Data Figure 7. Transcriptional Role of HDAC3 and ERRα in BAT

(a) Heat map demonstrating correlation of RNA-seq and GRO-seq data. Differentially expressed genes in RNA-seq or GRO-seq data were sorted by $\log_2$FC in RNA-seq. **(b)** *De novo* motif enrichment at repressed eRNAs in *Adipoq*-Cre, HDAC3 KO mice versus control littermates (n= 10, 10; pooled biological replicates/library) maintained at 22°C and ranked by *P*-value. **(c)** Endogenous HDAC3 co-immunoprecipitation of ERRα in differentiated mature brown adipocytes. **(d–e)** RT-qPCRs of BAT *Ucp1* eRNA expression and **(f)** *Ucp1* mRNA at 22°C and 29°C in *Adipoq*-Cre and *Ucp1*-Cre HDAC3 KO mice versus control littermates, 29°C (n= 9 *Adipoq*-Cre, 6 control; n= 5 *Ucp1*-Cre, 6 control) and 22°C (n= 9 *Adipoq*-Cre, 7 control; n= 5 *Ucp1*-Cre, 7 control). **(g)** ChIP-qPCR of ERRα at *Ucp1* enhancers in *Adipoq*-Cre HDAC3 KO versus control littermates (n= 3, 3) adapted to 29°C. **(h)** RT-qPCR of *ERRα* and *Ucp1* mRNA expression and **(i)** *Ucp1* eRNA expression in ERRα KO BAT versus control littermates (n= 8, 7). **(j)** RT-qPCR analysis of *ERRα* and *Ucp1* mRNA expression in mature brown adipocytes following siRNA mediated knockdown of *ERRα* versus scramble 72 h post-transfection (n= 3, 3). *P<0.05, **P<0.01, ***P<0.001 as determined by a two-tailed Student's t-test (d–e, g–j), two-way ANOVA with Holm-Sidak's post-test (f). *P*-values for motif enrichment as determined by binomial test (b). Data are represented as mean ± s.e.m.

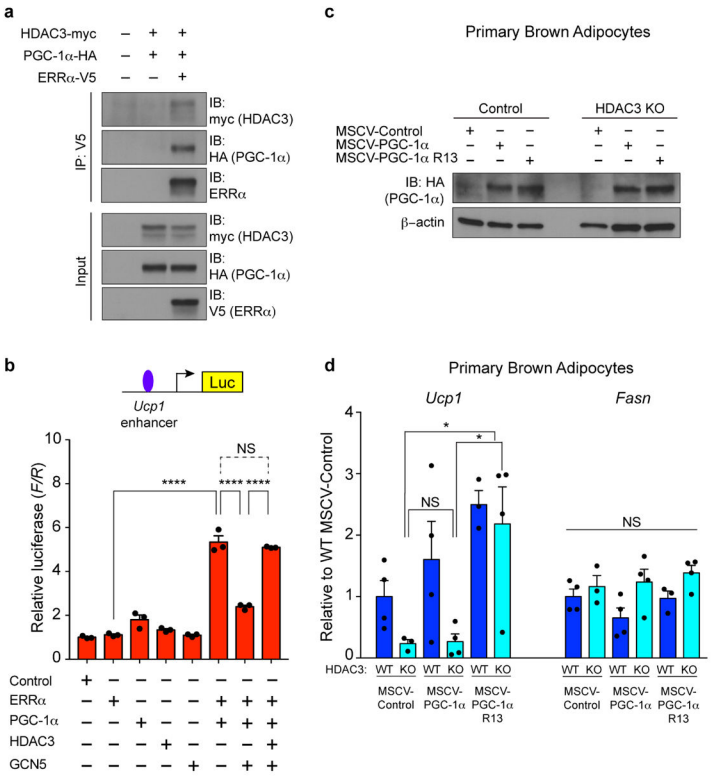

Extended Data Figure 8. Role of HDAC3 on PGC-1α acetylation and function

(a) Co-immunoprecipitation of HDAC3 and PGC-1α with ERRα from 293FT cells. **(b)** Luciferase reporter assay of transcription driven by the major *Ucp1* enhancer (−6 kb) following transfection of ERRα, PGC-1α**,** GCN5, and/or HDAC3 (n= 3 replicates per condition). **(c–d)** Primary brown pre-adipocytes from *Rosa26*-CreER-positive HDAC3$^{F/F}$ and HDAC3$^{F/F}$ control littermates transduced with MSCV retroviruses: Control, PGC-1α WT, or non-acetylatable PGC-1α R13 mutant, and treated with 2μm 4-OHT during days 0–2 of differentiation to deplete HDAC3, and studied at Day 8 of differentiation. **(c)** Immunoblot analysis of exogenous PGC-1α expression in primary brown adipocytes (n= 2 replicates pooled per lane). **(d)** RT-qPCR analysis of *Ucp1* and *Fasn* expression in control and HDAC3 KO primary brown adipocytes following transduction with MSCV-Control (n= 4 control, 3 HDAC3 KO), MSCV-PGC-1α WT (n= 4 control, 4 HDAC3 KO), or MSCV-PGC-1α R13 (non-acetylatable mutant) (n= 3 Control, 4 HDAC3 KO). *P<0.05, **P<0.01, ***P<0.001, ****P<0.0001, as determined by a one-way ANOVA and a Tukey's post-test (b, d). Data are represented as mean ± s.e.m.

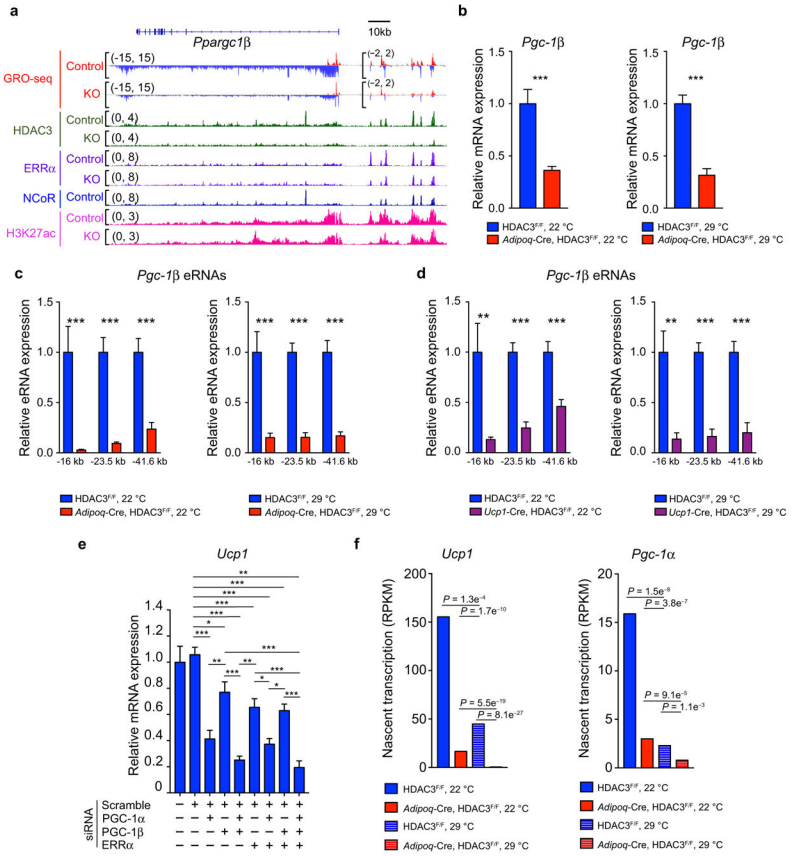

Extended Data Figure 9. HDAC3 and ERRα activate *Ppargc1β* enhancers and transcription

(a) Genome browser tracks of the *Ppargc1β* locus highlighting GRO-seq and ChIP-seq data from HDAC3 KO and control BAT (y-axis scales, normalized reads, reads per million) demonstrating co-binding of HDAC3, ERRα, and NCoR at functional enhancers. **(b)** BAT PGC-1*β* mRNA levels in *Adipoq*-Cre HDAC3 KO BAT versus control littermates (29°C: n= 9, 6; 22°C, n= 9, 7). **(c–d)** RT-qPCR of eRNAs found at HDAC3 and ERRα enhancers in *Adipoq*-Cre HDAC3 KO BAT versus control littermates (29°C: n= 9, 6; 22°C, n= 9, 7) and *Ucp1*-Cre HDAC3 KO BAT versus control littermates (29°C: n= 5, 6; 22°C, n= 5, 7). **(e)** RT-qPCR analysis of *Ucp1* mRNA expression in mature brown adipocytes following combinatorial siRNA knockdown of *Pgc-1*α, *Pgc-1*β and/or ERRα versus scramble siRNA (n= 5 replicates per condition). Statistical analysis performed amongst groups transfected with siRNAs. **(f)** Quantification of *Ucp1* and *Pgc-1*a nascent gene body transcription (GRO-seq) at 22°C and 29°C in *Adipoq*-Cre HDAC3 KO BAT versus control littermates (n= 10, 10, pooled biological replicates per library). **P*<0.05, ***P*<0.01, ****P*<0.001, as determined by a two-tailed Student's *t*-test (b–d), one-way ANOVA and a Holm-Sidak's post-test (e) or an exact test (performed in EdgeR). Data are represented as mean ± s.e.m.

Supplementary Material

Refer to Web version on PubMed Central for supplementary material.

Acknowledgments

We thank the Next-Generation Sequencing Core and the Mouse Phenotyping, Physiology and Metabolism Core of the Penn Diabetes Research Center (NIH P30 DK19525). This work was supported by NIH R01 DK45586 (M.A.L.), NIH F30 DK104513 (M.J.E.), and the JPB Foundation.

References

1. Cannon B, Nedergaard J. Brown adipose tissue: function and physiological significance. Physiol Rev. 2004; 84:277–359. [PubMed: 14715917]
2. Guenther MG, Barak O, Lazar MA. The SMRT and N-CoR Corepressors Are Activating Cofactors for Histone Deacetylase 3. Mol Cell Biol. 2001; 21:6091–6101. [PubMed: 11509652]
3. Chouchani ET, et al. Mitochondrial ROS regulate thermogenic energy expenditure and sulfenylation of UCP1. Nature. 2016; 532:112–6. [PubMed: 27027295]
4. Enerbäck S, et al. Mice lacking mitochondrial uncoupling protein are cold-sensitive but not obese. Nature. 1997; 387:90–94.
5. Ukropec J, Anunciado RP, Ravussin Y, Hulver MW, Kozak LP. UCP1-independent thermogenesis in white adipose tissue of cold-acclimated Ucp1−/− mice. J Biol Chem. 2006; 281:31894–31908. [PubMed: 16914547]
6. Bal NC, et al. Sarcolipin is a newly identified regulator of muscle-based thermogenesis in mammals. Nat Med. 2012; 18:1575–9. [PubMed: 22961106]
7. Kazak L, et al. A Creatine-Driven Substrate Cycle Enhances Energy Expenditure and Thermogenesis in Beige Fat. Cell. 2015; 163:643–655. [PubMed: 26496606]
8. Long JZ, et al. The Secreted Enzyme PM20D1 Regulates Lipidated Amino Acid Uncouplers of Mitochondria. Cell. 2016; 166:424–435. [PubMed: 27374330]
9. Harms M, Seale P. Brown and beige fat: development, function and therapeutic potential. Nat Med. 2013; 19:1252–63. [PubMed: 24100998]
10. Loft A, Forss I, Mandrup S. Genome-Wide Insights into the Development and Function of Thermogenic Adipocytes. Trends Endocrinol Metab. 2017; 28:104–120. [PubMed: 27979331]
11. Chen L, Fischle W, Verdin E, Greene WC. Duration of nuclear NF-kappaB action regulated by reversible acetylation. Science. 2001; 293:1653–1657. [PubMed: 11533489]
12. Bhaskara S, et al. Deletion of Histone Deacetylase 3 Reveals Critical Roles in S Phase Progression and DNA Damage Control. Mol Cell. 2008; 30:61–72. [PubMed: 18406327]
13. Sun Z, et al. Hepatic Hdac3 promotes gluconeogenesis by repressing lipid synthesis and sequestration. Nat Med. 2012; 18:934–42. [PubMed: 22561686]
14. Mullican SE, et al. Histone deacetylase 3 is an epigenomic brake in macrophage alternative activation. Genes Dev. 2011; 25:2480–2488. [PubMed: 22156208]
15. Hoeksema, Ma, et al. Targeting macrophage Histone deacetylase 3 stabilizes atherosclerotic lesions. EMBO Mol Med. 2014; 6:e201404170.
16. Razidlo DF, et al. Histone deacetylase 3 depletion in osteo/chondroprogenitor cells decreases bone density and increases marrow fat. PLoS One. 2010; 5
17. Alenghat T, et al. Histone deacetylase 3 coordinates commensal-bacteria-dependent intestinal homeostasis. Nature. 2013; 504:153–157. [PubMed: 24185009]
18. Montgomery RL, et al. Maintenance of cardiac energy metabolism by histone deacetylase 3 in mice. J Clin Invest. 2008; 118:3588–3597. [PubMed: 18830415]
19. Sun Z, et al. Diet-induced lethality due to deletion of the Hdac3 gene in heart and skeletal muscle. J Biol Chem. 2011; 286:33301–33309. [PubMed: 21808063]
20. Rada-Iglesias A, et al. A unique chromatin signature uncovers early developmental enhancers in humans. Nature. 2011; 470:279–83. [PubMed: 21160473]
21. Core LJ, Waterfall JJ, Lis JT. Nascent RNA sequencing reveals widespread pausing and divergent initiation at human promoters. Science. 2008; 322:1845–8. [PubMed: 19056941]
22. Fang B, et al. Circadian enhancers coordinate multiple phases of rhythmic gene transcription in vivo. Cell. 2014; 159:1140–1152. [PubMed: 25416951]

23. Wang D, et al. Reprogramming transcription by distinct classes of enhancers functionally defined by eRNA. Nature. 2011; 474:390–4. [PubMed: 21572438]
24. Gerhart-Hines Z, et al. The nuclear receptor Rev-erbα controls circadian thermogenic plasticity. Nature. 2013; 503:410–3. [PubMed: 24162845]
25. Giguère V. Transcriptional control of energy homeostasis by the estrogen-related receptors. Endocrine Reviews. 2008; 29:677–696. [PubMed: 18664618]
26. Soccio RE, et al. Genetic Variation Determines PPARγ Function and Anti-diabetic Drug Response in Vivo. Cell. 2015; 162:33–44. [PubMed: 26140591]
27. Rajakumari S, et al. EBF2 determines and maintains brown adipocyte identity. Cell Metab. 2013; 17:562–574. [PubMed: 23499423]
28. Dixen K, et al. ERRγ enhances UCP1 expression and fatty acid oxidation in brown adipocytes. Obesity. 2013; 21:516–524. [PubMed: 23404793]
29. Rodgers JT, Lerin C, Gerhart-Hines Z, Puigserver P. Metabolic adaptations through the PGC-1 alpha and SIRT1 pathways. FEBS Lett. 2008; 582:46–53. [PubMed: 18036349]
30. Uldry M, et al. Complementary action of the PGC-1 coactivators in mitochondrial biogenesis and brown fat differentiation. Cell Metab. 2006; 3:333–341. [PubMed: 16679291]
31. Mullican SE, et al. A novel adipose-specific gene deletion model demonstrates potential pitfalls of existing methods. Mol Endocrinol. 2013; 27:127–34. [PubMed: 23192980]
32. Luo J, et al. Reduced fat mass in mice lacking orphan nuclear receptor estrogen-related receptor alpha. Mol Cell Biol. 2003; 23:7947–56. [PubMed: 14585956]
33. Cannon B, Nedergaard J. Nonshivering thermogenesis and its adequate measurement in metabolic studies. J Exp Biol. 2011; 214:242–253. [PubMed: 21177944]
34. Pecinová A, Drahota Z, Nůsková H, Pecina P, Houštěk J. Evaluation of basic mitochondrial functions using rat tissue homogenates. Mitochondrion. 2011; 11:722–728. [PubMed: 21664301]
35. Picard M, et al. Mitochondrial structure and function are disrupted by standard Isolation methods. PLoS One. 2011; 6
36. Houstek J, Cannon B, Lindberg O. Glycerol-3-Phosphate Shuttle and Its function in intermediary metabolism of hamster brown adipose tissue. Eur J Biochem. 1975; 54:11–18. [PubMed: 168075]
37. Wang H, et al. Resveratrol Rescues Kidney Mitochondrial Function Following Hemorrhagic Shock. Shock. 2015; 44:173–80. [PubMed: 25895148]
38. Porter C, et al. Human and Mouse Brown Adipose Tissue Mitochondria Have Comparable UCP1 Function. Cell Metab. 2016; 24:246–255. [PubMed: 27508873]
39. Feng D, et al. A Circadian Rhythm Orchestrated by Histone Deacetylase 3 Controls Hepatic Lipid Metabolism. Science (80-). 2011; 331:1315–1319.
40. Harms MJ, et al. Prdm16 is required for the maintenance of brown adipocyte identity and function in adult mice. Cell Metab. 2014; 19:593–604. [PubMed: 24703692]
41. Kim D, et al. TopHat2: accurate alignment of transcriptomes in the presence of insertions, deletions and gene fusions. Genome Biol. 2013; 14:R36. [PubMed: 23618408]
42. Liao Y, Smyth GK, Shi W. FeatureCounts: An efficient general purpose program for assigning sequence reads to genomic features. Bioinformatics. 2014; 30:923–930. [PubMed: 24227677]
43. Robinson MD, McCarthy DJ, Smyth GK. edgeR: a Bioconductor package for differential expression analysis of digital gene expression data. Bioinformatics. 2010; 26:139–40. [PubMed: 19910308]
44. Chen EY, et al. Enrichr: interactive and collaborative HTML5 gene list enrichment analysis tool. BMC Bioinformatics. 2013; 14:128. [PubMed: 23586463]
45. Kuleshov MV, et al. Enrichr: a comprehensive gene set enrichment analysis web server 2016 update. Nucleic Acids Res. 2016; gkw377. doi: 10.1093/nar/gkw377
46. Eyre TA, et al. The HUGO Gene Nomenclature Database, 2006 updates. Nucleic Acids Res. 2006; 34:D319–D321. [PubMed: 16381876]
47. Kent WJ, Zweig aS, Barber G, Hinrichs aS, Karolchik D. BigWig and BigBed: enabling browsing of large distributed datasets. Bioinformatics. 2010; 26:2204–7. [PubMed: 20639541]
48. Quinlan AR, Hall IM. BEDTools: a flexible suite of utilities for comparing genomic features. Bioinformatics. 2010; 26:841–2. [PubMed: 20110278]

49. Using the SRA Toolkit to convert .sra files into other formats. SRA Knowledge Base. 2011
50. Thorvaldsdóttir H, Robinson JT, Mesirov JP. Integrative Genomics Viewer (IGV): High-performance genomics data visualization and exploration. Brief Bioinform. 2013; 14:178–192. [PubMed: 22517427]
51. Robinson JT, et al. Integrative genomics viewer. Nat Biotechnol. 2011; 29:24–26. [PubMed: 21221095]
52. Langmead B, Trapnell C, Pop M, Salzberg SL. Ultrafast and memory-efficient alignment of short DNA sequences to the human genome. Genome Biol. 2009; 10:R25. [PubMed: 19261174]
53. Heinz S, et al. Simple combinations of lineage-determining transcription factors prime cis-regulatory elements required for macrophage and B cell identities. Mol Cell. 2010; 38:576–89. [PubMed: 20513432]
54. Dunham I, et al. An integrated encyclopedia of DNA elements in the human genome. Nature. 2012; 489:57–74. [PubMed: 22955616]
55. Harms MJ, et al. PRDM16 binds MED1 and controls chromatin architecture to determine a brown fat transcriptional program. Genes Dev. 2015; 29:298–307. [PubMed: 25644604]
56. Martin M. Cutadapt removes adapter sequences from high-throughput sequencing reads. EMBnet journal. 2011; 17:10.
57. Ritchie ME, et al. Limma powers differential expression analyses for RNA-sequencing and microarray studies. Nucleic Acids Res. 2015; 43:e47. [PubMed: 25605792]
58. Robinson MD, Smyth GK. Small-sample estimation of negative binomial dispersion, with applications to SAGE data. Biostatistics. 2008; 9:321–332. [PubMed: 17728317]
59. Step SE, et al. Anti-diabetic rosiglitazone remodels the adipocyte transcriptome by redistributing transcription to PPAR-driven enhancers. Genes Dev. 2014; 28:1018–1028. [PubMed: 24788520]

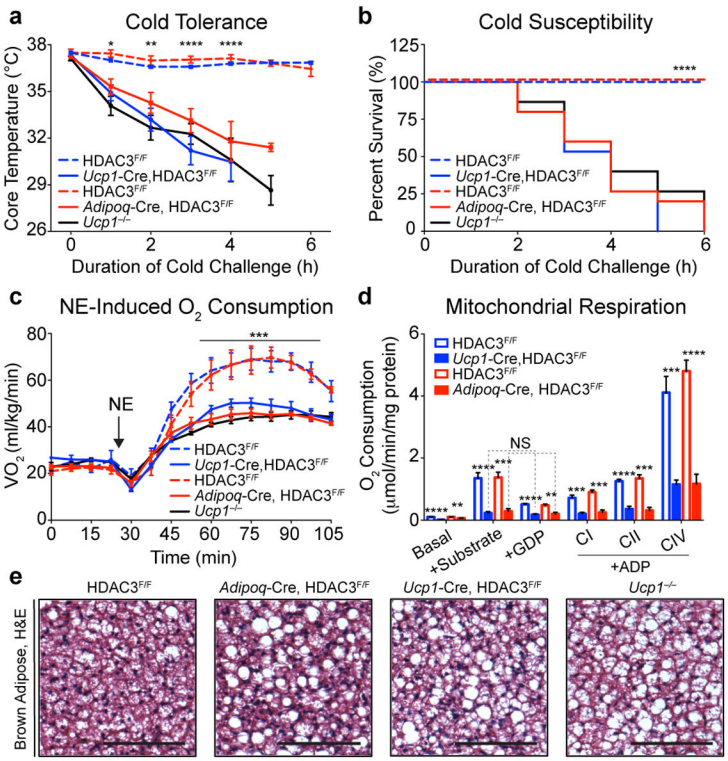

Figure 1. HDAC3 controls BAT thermogenesis

(a, b) Effect of acute cold exposure from standard housing at 22°C to 4°C on *Adipoq*-Cre HDAC3 knockout (KO) mice versus control littermates (n= 15, 8), *Ucp1*-Cre HDAC3 KO mice versus control littermates (n= 15, 7), and *Ucp1*$^{-/-}$ mice (n= 15): **a,** core body temperature; **b**, survival. **(c)** Oxygen consumption rates of anesthetized *Adipoq*-Cre HDAC3 KO mice versus control littermates (n= 12, 5), *Ucp1*-Cre HDAC3 KO mice versus control littermates (n= 6, 5), and *Ucp1*$^{-/-}$ mice (n= 5) following injection of 1 mg kg^{-1} norepinephrine. **(d)** Mitochondrial respiration of purified BAT homogenates from *Adipoq*-Cre HDAC3 KO mice versus control littermates (n= 5, 6), and *Ucp1*-Cre HDAC3 KO mice versus control littermates (n= 6, 5), following brief acclimation to thermoneutrality. Mitochondria were provided palmitoylcarnitine and pyruvate substrates. UCP1-dependent respiration was assessed upon addition of guanosine diphosphate (GDP), and coupled respiration rates of complex I, II, and IV were determined in the presence of adenosine diphosphate (ADP). **(e)** Representative hematoxylin and eosin staining of interscapular brown adipose from 10–12 week old mice at 22°C. Scale bars, 100µm. *P<0.05, **P<0.01, ***P<0.001, ****P<0.0001 as analyzed by two-way analysis of variance (ANOVA) and a Tukey's post-test (a,c), log-rank (Mantel-Cox) test (b), or two-tailed Student's t-test (d). Data are represented as mean ± s.e.m.

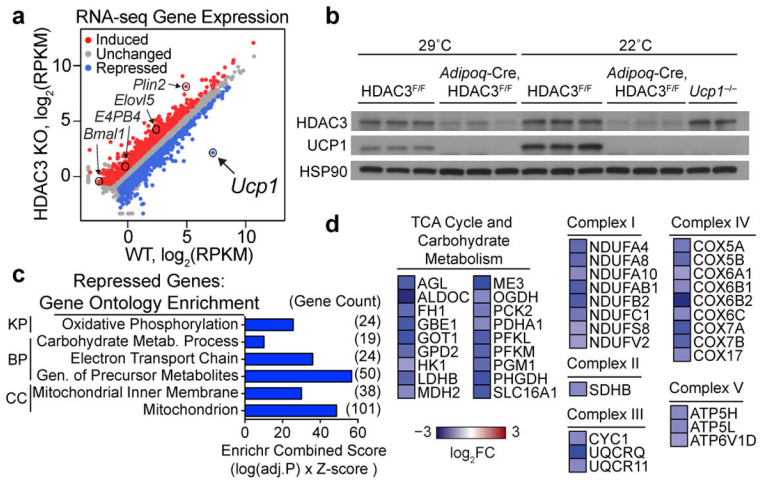

Figure 2. HDAC3 is required for expression of UCP1 and OXPHOS genes in BAT

(a) Scatterplot of RNA-seq data showing HDAC3 regulated BAT genes from *Adipoq*-Cre HDAC3 KO versus control littermates (n= 4, 4) adapted to thermoneutrality (fold-change > 1.5 up (red) or down (blue) and FDR < 0.01). RPKM, reads per kilobase per million. **(b)** Immunoblot from BAT of *Adipoq*-Cre HDAC3 KO, control littermates, or *Ucp1*$^{-/-}$ adapted to 29°C or maintained at 22°C (n= 3, 3; n= 3, 3; n= 2). **(c)** Gene ontology (GO) and pathway analysis of down-regulated genes identified by RNA-seq and selected by Enrichr combined score (KP, KEGG Pathway; BP, Biological Process; CC, Cellular Component). **(d)** Heat map depicting down-regulated genes identified in GO analysis.

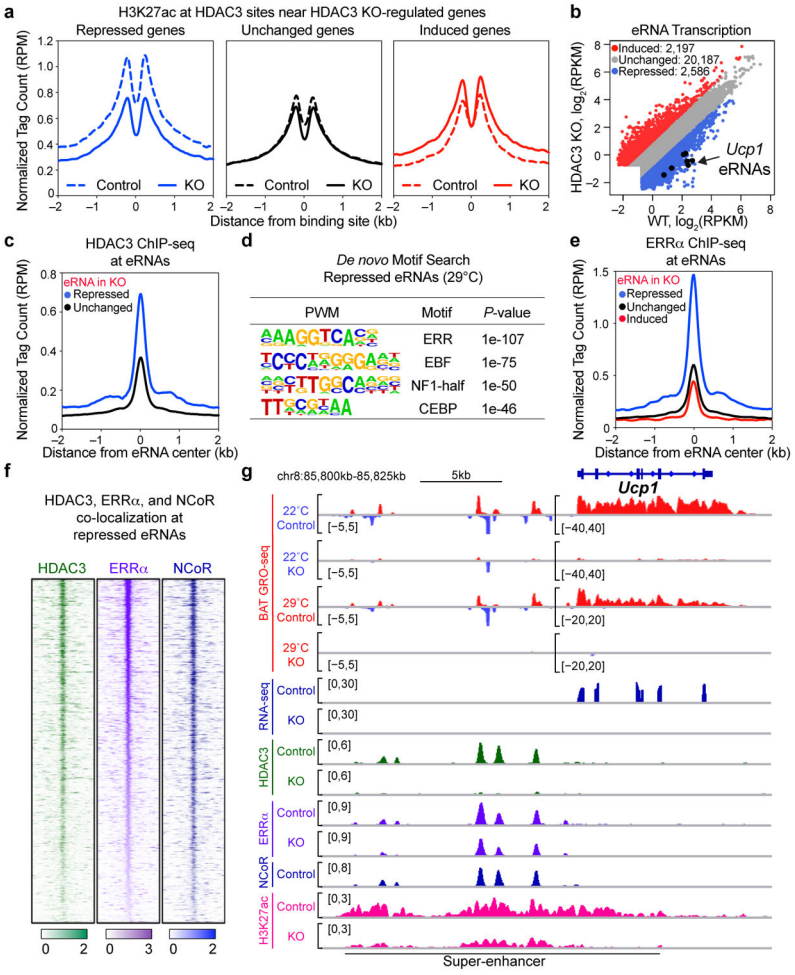

Figure 3. HDAC3 functions as an ERRα coactivator in BAT

(a) Average H3K27ac ChIP-seq profiles of *Adipoq*-Cre HDAC3 KO mice versus control littermates (n= 3, 3; pooled biological replicates/library) at enhancers bound by HDAC3 within 100 kb of transcription start sites of HDAC3 KO-regulated genes by GRO-seq (fold-change > 1.5 or < 0.5). Decreased H3K27ac at HDAC3 sites near repressed genes (N= 1085, $P = 1.0\times10^{-123}$) and increased H3K27ac at HDAC3 sites near induced genes (N= 897, $P = 9.0\times10^{-56}$) upon loss of HDAC3. **(b)** Scatter plot of enhancer RNAs (eRNAs) measured by GRO-seq in *Adipoq*-Cre HDAC3 KO mice versus control littermates (n= 10, 10; pooled biological replicates/library) at 29°C, highlighting induced and repressed eRNAs (Red, Fold-change > 2 & Blue, Fold-change < 0.5). **(c)** Average HDAC3 ChIP-seq profile of control littermates (n= 5, pooled biological replicates/library) at enhancers with repressed or unchanged eRNAs in HDAC3 KO. Significant HDAC3 binding found at HDAC3 KO-repressed eRNAs relative to unchanged eRNAs ($P = 2.4\times10^{-215}$). **(d)** *De novo* motif search at eRNA sites repressed in HDAC3 KO at 29°C (ranked by *P*-value). **(e)** Average ERRα ChIP-seq profile in control littermates (n= 5, pooled biological replicates/library) at enhancers with differential eRNAs in HDAC3 KO. Significant ERRα found at HDAC3 KO-repressed eRNAs relative to unchanged eRNAs ($P=1.0\times10^{-288}$). **(f)** Heat map depicting HDAC3, ERRα, and NCoR co-localization at enhancers with repressed eRNAs in HDAC3

KO mice. **(g)** Genome browser tracks of the *Ucp1* super-enhancer locus highlighting GRO-seq (22°C, 29°C), RNA-seq (29°C), and ChIP-seq (29°C) data (y-axis scales in brackets: reads per million (RPM); eRNA tracks feature adjusted y-axis scale). *P*-values for ChIP-seq or motif search determined by Wilcoxon or binomial test, respectively.

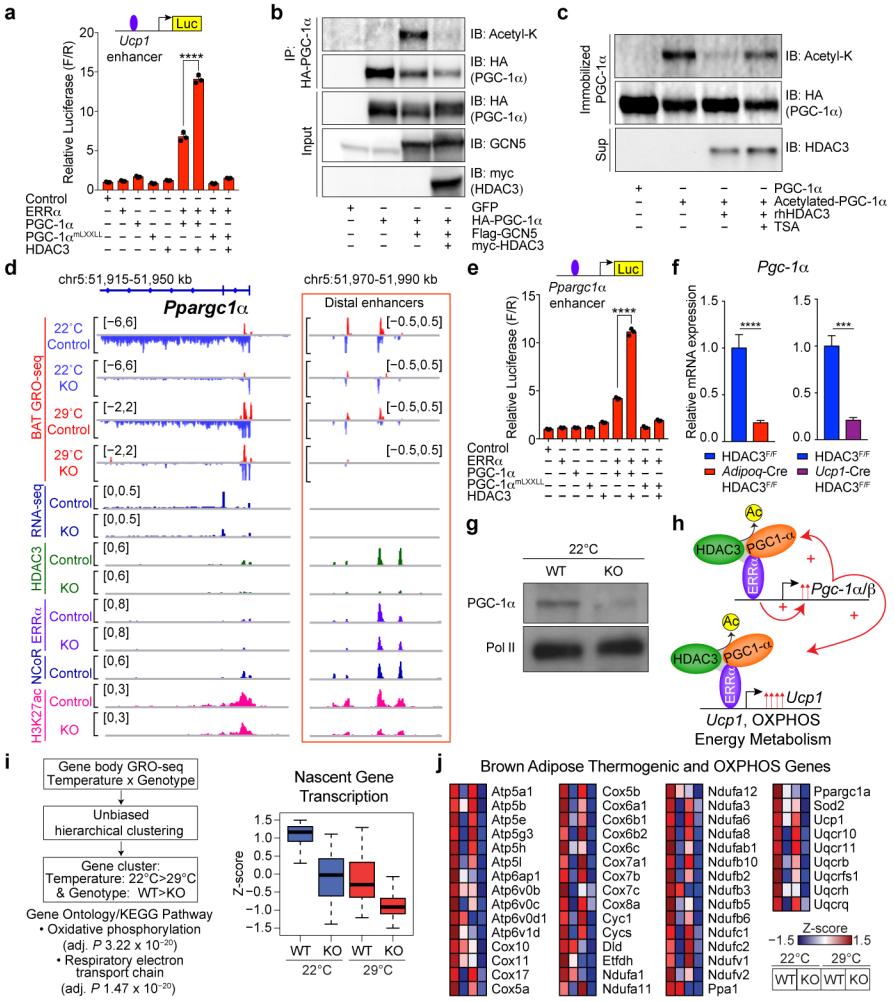

Figure 4. HDAC3 coactivation of ERRα is mediated by PGC-1α deacetylation

(a) Luciferase reporter assay of transcription driven by an identified *Ucp1* enhancer (−6 kb), demonstrating effects of ERRα, HDAC3, wild type PGC-1α, and/or a PGC-1α LXXLL mutant (L1/2/3A) unable to interact with ERRα (n= 3 replicates/condition). **(b)** Immunoblot analysis of PGC-1α lysine acetylation following immunoprecipitation from co-transfected 293FT cells. **(c)** Immunoblot analysis of an *in vitro* deacetylation reaction of purified acetylated-PGC-1α by recombinant human HDAC3, with or without trichostatin A (TSA). **(d)** Genome browser tracks of the *Ppargc1α* locus highlighting GRO-seq and RNA-seq data, and eRNAs at HDAC3, ERRα, and NCoR co-bound distal enhancers (boxed). **(e)** Luciferase reporter assay as in (a) for identified *Ppargc1α* distal enhancer (−38 kb), (n= 3 replicates/condition). **(f)** BAT *Pgc-1α* mRNA from *Adipoq*-Cre HDAC3 KO mice versus control littermates (n= 9, 6) and *Ucp1*-Cre HDAC3 KO mice versus control littermates (n= 5, 6). **(g)** Immunoblot of PGC-1α in BAT nuclear extract of *Adipoq*-Cre HDAC3 KO versus control littermates (n= 5, 5 pooled replicates per lane). **(h)** BAT HDAC3 deacetylates PGC-1*α* to co-activate an ERR-driven transcriptional loop of *Ppargc1α/β Ucp1,* and OXPHOS genes. **(i)** Flow chart depicting unbiased hierarchical gene clustering of GRO-seq gene transcription by temperature and genotype. Boxplot displays gene cluster requiring HDAC3 coactivator

function, where line denotes median, top/bottom of boxes represents first/third quartiles, and whiskers denote 1.5x the interquartile range from first/third quartiles. **(j)** Heatmap of thermogenic and OXPHOS genes identified in (i). ***$P<0.001$, ****$P<0.0001$ as determined by one-way ANOVA with multiple comparisons and a Tukey's post-test (a, e) or two-tailed Student's *t*-test (f). Data are represented as mean ± s.e.m.